

# **The start-up phase of the PRACLAY Heater test**

A. Dizier, G. Chen, X.L. Li, J. Leysen,  
J. Verstricht, I. Troullinos, J. Rypens

EURIDICE Report, ref. EUR\_PH\_16\_025

2016

This report was written by A. Dizier (EIG EURIDICE), G. Chen (EIG EURIDICE), X.L. Li (EIG EURIDICE), J. Leysen. (EIG EURIDICE), J. Verstricht (EIG EURIDICE), I. Troullinos (EIG EURIDICE) and J. Rypens (EIG EURIDICE).

It was reviewed by S. Levasseur (ONDRAF/NIRAS) and X. Sillen (ONDRAF/NIRAS), approved by P. De Preter (EIG EURIDICE), and designed and produced by Bailleul Ontwerpbureau.

Contact person at EIG EURIDICE: Xiang Ling Li xli@euridice.be

Contact person at ONDRAF/NIRAS: Séverine Levasseur s.levasseur@nirond.be

Publisher: Peter De Preter, Sneppenstraat 66, 3010 Kessel-Lo

**EIG EURIDICE**  
**Boeretang 200**  
**BE-2400 MOL**  
**Tel. +32 14 33 27 84**  
**[www.euridice.be](http://www.euridice.be)**

The data, results, conclusions and recommendations contained in this report are the property of EIG EURIDICE. This publication may be not quoted without acknowledgement of the source. It is made available on the basis that it will not be used for commercial purposes. All commercial uses, including copying and re-publication, require prior written authorisation from EIG EURIDICE.

<b>Document Datasheet</b>			
Title <b>The start-up phase of the PRACLAY Heater test</b>			
Author(s) of the document <b>A. Dizier (EIG EURIDICE), G. Chen (EIG EURIDICE), X.L. Li (EIG EURIDICE), J. Leysen. (EIG EURIDICE), J. Verstricht (EIG EURIDICE), I. Troullinos (EIG EURIDICE), J. Rypens (EIG EURIDICE)</b>		Reviewer(s) of the document <b>S��verine Levasseur (ONDRAF/NIRAS) Xavier Sillen (ONDRAF/NIRAS)</b> English language reviewed by <b>Moira Bluer</b>	
Series	<b>NA</b>	Publication date	<b>2 May 2016</b>
Document type	<b>EURIDICE REPORT</b>	Review status	<b>Version 1</b>
Status	<b>Public</b>	Revision number	<b>0</b>
EURIDICE number of report	<b>16-025</b>	Subcontractor reference number	<b>NA</b>
ISBN	<b>NA</b>	Total number of pages	<b>63</b>
Approver(s) of the document <b>Peter De Preter (EIG EURIDICE)</b>			

<b>EURIDICE approval</b>	<b>Date</b>	<b>Sign</b>
Author: <b>Arnaud Dizier</b>	18/4/2016	
Reviewer: <b>S��verine Levasseur</b>	18/4/2016	
Approver: <b>Peter De Preter</b>	18/4/2016	



## Summary

In Belgium, geological disposal in poorly indurated clay is proposed for the long-term management of high-level and/or long-lived radioactive waste. High-level radioactive waste produces heat. After disposal, following a cooling period of 60 years on the surface, this heat will have an impact on the thermo-hydro-mechanical behaviour of the clay for a limited period of time (approximately 1,000 years).

In the HADES underground research laboratory in Mol, Belgium, the large-scale PRACLAY Heater test is being carried out by EIG EURIDICE as part of the research programme of ONDRAF/NIRAS on geological disposal. The main goal of the PRACLAY Heater test is to examine the combined impact of hydro-mechanical disturbances caused by gallery construction and a large-scale thermal load on the Boom Clay due to heat-emitting high-level waste. This combined mechanical and thermal load leads to perturbations in the clay. In this respect, it must be verified that poorly indurated clays can retain their ability to physically contain radioactive substances after these perturbations and that the performance of this important natural barrier will thus not be significantly altered.

The thermo-hydro-mechanical response of the Boom Clay has already been investigated in laboratory tests and during the small-scale in-situ ATLAS experiments. To confirm and if necessary refine the existing knowledge and models of the thermo-hydro-mechanical behaviour of the Boom Clay, the PRACLAY Heater test is being performed on a scale and in conditions that are representative of a real repository.

The Heater test is installed in the PRACLAY gallery. A 30-metre section of this gallery is being heated for 10 years, maintaining a constant temperature of 80°C at the interface between the concrete lining and the Boom Clay. This target temperature is slightly higher than the temperature that is expected in a real repository. The heated part of the gallery is separated from the non-heated part by a seal made of a bentonite ring supported by a cylindrical steel structure. Bentonite was chosen as seal material because of its swelling capacity upon hydration and its intrinsic low permeability. Due to its swelling capacity, the seal hydraulically cuts off the heated part from the non-heated part of the gallery. Together with a water-saturated backfill in the heated part of the gallery, the seal ensures quasi-undrained boundary conditions for the experiment.

On 3 November 2014, the heating system was switched on and the target temperature of 80°C was reached on 19 August 2015. These two dates define the start-up phase of the experiment. To reach this target temperature, three heating phases were applied: the first at a linear thermal load density of 250 W per metre of gallery, the second at 350 W/m and the third at 450 W/m. The evolution of the experiment is continuously monitored by instruments installed in the different parts of the test set-up and in an extensive network of instrumented boreholes in the surrounding clay. In general, the different components of the experiment reacted to heating in line with EURIDICE's expectations, which were largely based on numerical simulations.

Inside the saturated PRACLAY gallery backfill, the temperature and pore water pressure immediately started to increase after the heating system was switched on. The pore water pressure rose from 1 MPa just before the start of heating to 2.9 MPa at the end of the start-up phase.

In the Boom Clay, the transfer of heat caused an increase in temperature and pore water pressure. An extension of the thermally affected zone of about 10 m around the PRACLAY gallery was observed at the end of the start-up phase. The hydraulically affected zone, defined by pore water pressure changes, is larger, extending from 10 to up to 15 m around the PRACLAY gallery.

The different observations leave no doubt about the performance of the seal. It effectively fulfils its role of hydraulic cut-off between the heated and non-heated parts, avoiding dissipation of pore water pressure from the heated part towards the non-heated part of the experiment.

The observations were compared with the blind predictions of a 2D Axisymmetric and a 2D Plane strain model. The comparisons show that the observed temperature and pore water pressure variations correspond quite well with the blind predictions, both in the gallery and in the Boom Clay. Deviations between the measurements and the predictions of temperature in horizontal or upward boreholes are almost certainly related to the presence of open boreholes, allowing a potential heat transfer by convection in the casing. This results in a modification of the temperature field around the boreholes. For the seal, larger discrepancies between the measurements and the modelling were observed. A more detailed analysis of the complex seal behaviour will be carried out in the future course of the experiment. The conclusions of this first comparison of the measurements with the numerical results give us an initial indication of how and where to improve the models used for the future follow-up of the experiment during the ten-year heating phase at a constant temperature at the interface with the Boom Clay.

Overall, it can be stated that the first phase of the experiment is a success. The experimental set-up was found to be reliable and the whole system generally evolved as expected during the start-up phase. Since the end of the start-up phase, the temperature at the interface between the lining and the Boom Clay has remained constant at 80°C.

# Table of contents

<b>1.</b>	<b>Introduction .....</b>	<b>9</b>
1.1.	Background .....	9
1.2.	Goals and design of the PRACLAY Heater test.....	11
1.3.	Goal and structure of this report.....	13
<b>2.</b>	<b>Experimental set-up .....</b>	<b>14</b>
2.1.	Heating system .....	14
2.2.	Hydraulic seal.....	16
2.3.	Backfill sand.....	17
2.4.	Instrumentation and monitoring system.....	17
2.5.	Data Acquisition system.....	21
<b>3.</b>	<b>Test evolution.....</b>	<b>22</b>
3.1.	Temperature in the concrete lining and at the lining/Boom Clay interface.....	23
3.2.	Backfill pore water pressure.....	25
3.3.	Boom Clay responses.....	26
3.3.1.	Observations around Ring 50 of the PRACLAY gallery.....	26
3.3.2.	Temperature and pore water pressure profiles at other rings along the PRACLAY gallery .....	32
3.3.3.	Temperature and pore water pressure profiles in boreholes drilled from the Connecting gallery.....	35
3.3.4.	Comparison between PG50S and the Connecting gallery boreholes .....	37
3.4.	Responses in the bentonite seal .....	39
3.5.	Responses in the concrete lining.....	43
3.6.	Summary .....	46
<b>4.</b>	<b>Comparison with numerical modelling (blind predictions) .....</b>	<b>47</b>
4.1.	Description of the two numerical models .....	47
4.2.	Comparison with the observations .....	50
4.2.1.	Test-control parameters.....	50
4.2.2.	Observations in the Boom Clay .....	53
4.2.3.	Observations in the seal and concrete lining structures .....	56
4.3.	Summary and future work.....	59
<b>5.</b>	<b>Conclusions.....</b>	<b>60</b>
<b>6.</b>	<b>References .....</b>	<b>62</b>



# 1. Introduction

## 1.1. Background

For the long-term management of high-level and/or long-lived radioactive waste (categories B&C), ONDRAF/NIRAS, which is responsible for the management of radioactive waste in Belgium, proposes geological disposal in poorly indurated clay formations.

Research on geological disposal in clay started in Belgium more than 40 years ago. In 1974, the Belgian nuclear research centre SCK•CEN decided to construct an underground research facility in the Boom Clay to study the behaviour and characteristics of this clay below ground level and to test different techniques for excavating and constructing galleries in poorly indurated clay. The Boom Clay formation lies between 190 and 290 metres under the SCK•CEN site. The underground research facility, which is situated at a depth of 225 metres, is known as the HADES URL (Figure 1-1). The first part of HADES was constructed manually during the 1980s. EIG PRACLAY, an economic interest grouping between ONDRAF/NIRAS and SCK•CEN, was created in 1995 to carry out the PRACLAY project. The aim of the PRACLAY project was to demonstrate the feasibility of the geological disposal concept for high-level radioactive waste. This was done stepwise. First, in 2002/2003, an 80-metre-long gallery, called the Connecting gallery (CG) was constructed using an industrial tunnelling machine, connecting the second shaft with the existing part of the HADES laboratory. Then, in 2007, the PRACLAY gallery (PG) was constructed, perpendicularly connected with the Connecting gallery.

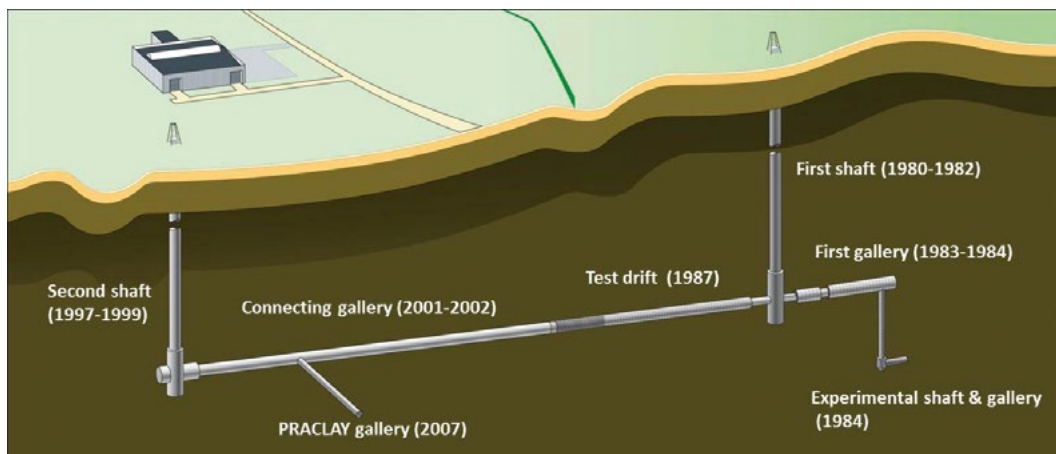


Figure 1-1: Construction history and layout of the HADES underground research laboratory

During the excavation and construction of these galleries, the hydro-mechanical behaviour of the Boom Clay was studied in detail and documented in the CLIPEX (2003) and SELFRAC (2007) reports. The main conclusion of these studies is that the Boom Clay displays highly coupled hydro-mechanical behaviour and has a self-sealing capacity, which means, for example, that the initial low permeability of the clay that is affected by the excavation gradually recovers.

High-level radioactive waste gives off heat. Two specific waste forms are considered in the RD&D programme on geological disposal: vitrified waste resulting from reprocessing and spent fuel. In Belgium, spent fuel assemblies are stored on the sites of the nuclear power plants at Doel and Tihange, where they are cooled. After reprocessing, vitrified waste is stored in buildings belonging to Belgoprocess, a subsidiary of ONDRAF/NIRAS, to cool down over a period of 60 years.

After the cooling period, the high-level waste forms (two vitrified waste canisters or four spent fuel assemblies) will be placed in a carbon steel overpack surrounded by a concrete buffer and an outer stainless steel envelope. Together, these engineered barriers make up the so-called "Supercontainer". The Supercontainer is the current reference design for the disposal of high-level, heat-producing radioactive waste forms (Figure 1-2). After manufacturing, the Supercontainer will then be placed horizontally in the disposal galleries, which are supported by a concrete lining. Finally, the void space between the Supercontainer and the gallery lining will be backfilled, probably with a cement-based material. The Supercontainer has the key benefit that it is assembled on the surface and has adequate radiation shielding to enable it to be subsequently manipulated without the need for shielded handling equipment.

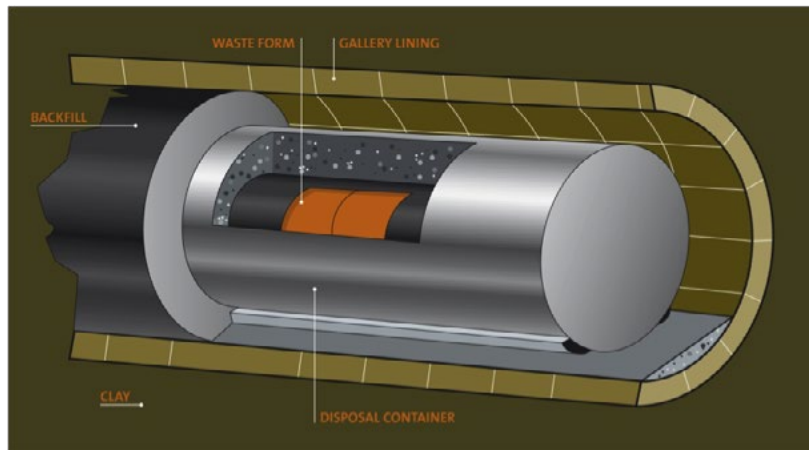


Figure 1-2: The Supercontainer design for vitrified waste as the reference for the Engineered Barrier System

After emplacement of the supercontainers in the disposal facility, the high-level radioactive waste will still produce some heat and will heat up the clay surrounding the disposal galleries.

To study the impact of this heat on the thermo-hydro-mechanical (THM) behaviour of the clay, a large number of on-surface laboratory tests have been performed (Horseman et al., 1987; Baldi et al., 1991; Sultan, 1997; Coll, 2005; Le, 2008; etc.). In addition, the smaller-scale in-situ ATLAS heater test was conducted in several phases in HADES from 1993 on (De Bruyn and Labat, 2002; Chen et al., 2011). The last phase of the ATLAS heater test (ATLAS IV) started on 18 October 2011. During the different phases of the ATLAS heater test, the temperature and pore water pressure response to thermal loading was measured in boreholes at a distance of several metres from the heated borehole. However, the set-up of the ATLAS heater test is more representative of the THM behaviour of the clay in the far field. The drilling-induced damaged zone of a borehole equipped with the heating element extends only a few centimetres around it, while the distance between the heating source and the measuring instruments is relatively large (several metres). The ATLAS experiment therefore resulted in a very good understanding of the THM behaviour of the Boom Clay in the far field of a repository, which was also achieved with numerical THM modelling.

Numerical simulations were performed to estimate the temperature increase in the Boom Clay around a disposal gallery containing spent fuel and vitrified high-level waste (Sillen and Marivoet, 2007), considering the Supercontainer as an engineered barrier system. The maximum temperature increase, as obtained from these simulations, amounts to 59°C for spent fuel and about 48°C for vitrified high-level waste and will be reached after 10 to 15 years. After this time, the clay will slowly cool down due to the diminishing heat production of the high-level radioactive waste. Figure 1-3 shows the temperature evolution at the interface between the Boom Clay and a disposal gallery. As the in-situ temperature of the Boom Clay is 16°C at the depth of the HADES URL, the maximum temperature at the clay/lining interface

of a disposal gallery would be 75°C for spent fuel and 64°C for vitrified high-level waste at this depth.

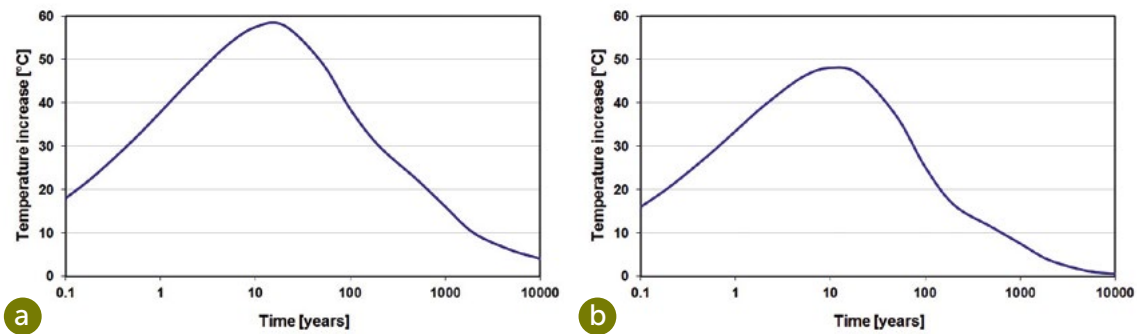


Figure 1-3: Temperature increase around a disposal gallery containing supercontainers with (a) spent fuel and (b) vitrified high-level radioactive waste

To confirm and refine the knowledge gained from these small-scale tests, on a scale and in conditions that are more representative of a real disposal facility, it was decided to perform a large-scale heating experiment in the PRACLAY gallery (PG), the so called “PRACLAY Heater test”. The background of the PRACLAY Heater test is described in more detail in the introductory part of the “The design and installation of the PRACLAY In-Situ Experiment” report by Van Marcke et al. (2013).

The ultimate goal of these small-scale and large-scale heater tests is to study the thermo-hydro-mechanical behaviour of the clay within the context of the research programme on geological disposal and to be sure that poorly indurated clay, such as the Boom Clay, retains its ability to physically contain radioactive substances when it is heated.

## 1.2. Goals and design of the PRACLAY Heater test

The main goal of the PRACLAY Heater test is to examine the combined impact of hydro-mechanical disturbances caused by gallery construction and a large-scale thermal load on the Boom Clay due to heat-emitting high-level waste (Van Marcke et al., 2013). Such a combined mechanical and thermal load leads to perturbations in the clay and can affect its performance as a host rock in the geological disposal concept for heat-emitting radioactive waste.

More specifically, the goals of the Heater test are to:

- confirm the thermal properties of the Boom Clay on a large scale and refine the models that describe the thermal evolution of the Boom Clay surrounding a disposal gallery containing heat-emitting radioactive waste;
- estimate the major consequences of the thermo-hydro-mechanical impact on the Boom Clay, particularly within the excavation-damaged zone (EDZ), focusing primarily on the mechanical damage and hydraulic conductivity;
- assess the long-term stability, under thermal conditions, of the concrete lining surrounding any waste package design, taking into account the temperature criterion of  $T_{max} < 100^{\circ}\text{C}$  around the primary waste package (Bel and Bernier, 2001);
- increase knowledge of the performance and reliability of monitoring devices under thermal stress and heat;
- assess the thermally and excavation-induced geochemical perturbations and their possible impact on radionuclide transport-related parameters; this is not a priority, however, and should not jeopardise achievement of the above objectives.

To cope with possible future changes in the repository design, the test was designed to be as design-independent as possible.

Simulating the exact THM conditions as in an actual repository is not possible. The time period over which the thermal load applies is too long (several hundreds or thousands of years (Sillen and Marivoet, 2006)), and also the length of the disposal galleries and the boundary conditions, such as the hydraulic conditions around the repository, are different. Since it is not possible to fully reproduce the timescale, the spatial scale and the boundary conditions of a real repository, the Heater test is being conducted under a well-controlled and reasonably conservative combination of thermal and hydraulic boundary conditions.

With respect to the thermal conditions, a 30-metre section of the PRACLAY gallery is being heated for 10 years at a constant temperature of 80°C at the interface between the concrete gallery lining and the clay, corresponding to a temperature increase of 64°C. This temperature is higher than would be expected in a high-level waste repository. As mentioned in 1.1., the maximum temperature at the interface between the gallery lining and the clay will be reached after 10 to 15 years, while in the PRACLAY Heater test, 80°C is attained within several months. In this regard, the test is on the conservative side compared with the temperature conditions in a real repository.

Attaining the most critical conditions in terms of the THM response of a disposal system within the limits of what is reasonably achievable implies quasi-undrained hydraulic boundary conditions, which maximises the fluid pressure increase resulting from thermal expansion of the pore water. In fact, an increase in pore fluid pressure within the natural barrier reduces the contact forces between the clay particles making up this barrier, reducing its strength and diminishing the mechanical stability of the repository. This required the installation of a hydraulic seal, with bentonite-based material, at the intersection between the heated and non-heated sections of the gallery and backfilling of the heated section with saturated sand. The installation of a hydraulic seal constituted the Seal Test, the main goal of which was to hydraulically seal the heated section of the gallery and its surrounding excavation-disturbed zone from the non-heated section. The hydraulic seal is purpose-built for the PRACLAY Heater test and is not representative of seals in a geological disposal repository.

The construction of the PRACLAY gallery and its crossing with the Connecting gallery constituted the Gallery and Crossing Test. The feasibility of excavating a gallery in the Boom Clay at a depth of 225 m using an industrial excavation technique had already been demonstrated in constructing the Connecting gallery. During the construction of the PRACLAY gallery, it was possible to optimise the excavation technique and further investigate the hydro-mechanical response of the Boom Clay to the excavation work.

The Gallery and Crossing Test, the Seal Test and the Heater Test together make up the PRACLAY In-Situ Experiment. A detailed description of all aspects of this experiment can be found in the EURIDICE report "The design and installation of the PRACLAY In-Situ Experiment" (Van Marcke et al., 2013).

### 1.3. Goal and structure of this report

On 3 November 2014, the heating system was switched on with an initial power of 250 W/m. Over the next nine months, the power of the heating system was increased stepwise. On 19 August 2015, an average temperature of 80°C was reached at the interface between the lining and the clay, marking the end of the start-up phase. The temperature will now be kept constant at 80°C for 10 years.

This report summarises the main observations of the start-up phase and an initial comparison with the modelling results that were obtained before the start of the Heater test (blind predictions). It does not contain a detailed interpretation or evaluation of the success criteria of the experiment. This will be done in future reports.

The report is composed of three main sections:

#### Experimental set-up

The first section briefly describes the different components constituting the Heater test, including the whole instrumentation and monitoring system to monitor the evolutions of the clay, and including the set-up of the seal.

#### Test evolution

This section provides an overview of all the observations in the Boom Clay, concrete lining and seal, from the first nine and a half months of the Heater test. The temperature and pore water pressure evolution as well as the profiles along boreholes are presented. Particular attention is devoted to the observations around Ring 50 of the PRACLAY gallery because of its central position in the heated area. Comparisons are also made between the boreholes at different locations in order to check the consistency and homogeneity of the results. The total pressure at different interfaces (Boom Clay/bentonite, Boom Clay/concrete lining) is also presented and discussed.

#### Comparison with the modelling

In the final section, all observations are compared with the modelling results. In the event of significant differences, the impact of these differences on the model used is discussed.

The modelling results that are used in this section have been obtained using the parameter values that were defined before the start of the heating phase (blind predictions). The conclusions drawn from these comparisons give us a roadmap for our future modelling efforts.

## 2. Experimental set-up

A quick overview of the main components of the PRACLAY Heater test is given in this section. The test set-up is mainly composed of a heating system and a hydraulic seal. The gallery is backfilled with sand and pressurised with water. The role of the seal is to hydraulically cut off the heated part from the non-heated part (Figure 2-1). Bentonite, an expansive clay with a high swelling potential under hydration, was chosen to achieve this goal. In this way the zone around the seal is sealed, which reduces the permeability around this zone (especially along the interface between the Boom Clay and the bentonite) and the high pressure inside the PRACLAY gallery is maintained.

The detailed specifications for the PRACLAY gallery, the hydraulic seal, the heater and the backfill material can be found in the EURIDICE report "The design and installation of the PRACLAY In-Situ Experiment" (Van Marcke et al., 2013).

At the end of this section, there is a brief description of the data acquisition system (DAQ) and of the different sensors used in the experiment.

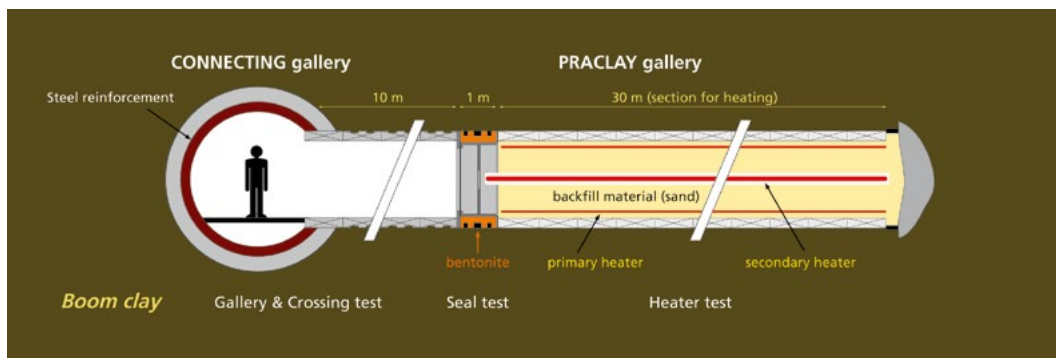


Figure 2-1: An overview of the PRACLAY In-Situ Experiment, including the components of the Heater test. The PRACLAY gallery has an inner radius of 0.95 m and the thickness of the lining is 30 cm.

### 2.1. Heating system

The heating system consists of a primary heater, attached to the gallery lining, and a secondary heater, which is placed in a central tube that rests on a support structure. Both of these are electrical heaters. Since the primary heater is inaccessible during the Heater test, twice as many primary heater cables than necessary have been installed (100% redundancy). The secondary heater is a back-up and will remain accessible and replaceable at all times during the test.

A control system regulating the heating power as a function of measured and target temperatures is also part of the heating system. During the start-up phase, the temperature was increased in a controlled manner to limit the thermal gradient over the gallery lining.

The primary heating system is divided into three zones as described in Figure 2-2:

- Zone 1: front-end zone, 2.26 m long, close to the PRACLAY seal,
- Zone 2: middle zone, 28.48 m long, in the middle of the experimental part of the gallery,
- Zone 3: far-end zone, 3.29 m long, at the end of the gallery.

Each zone comprises four heating sectors (sector 1 to 4), as shown in Figure 2-2.

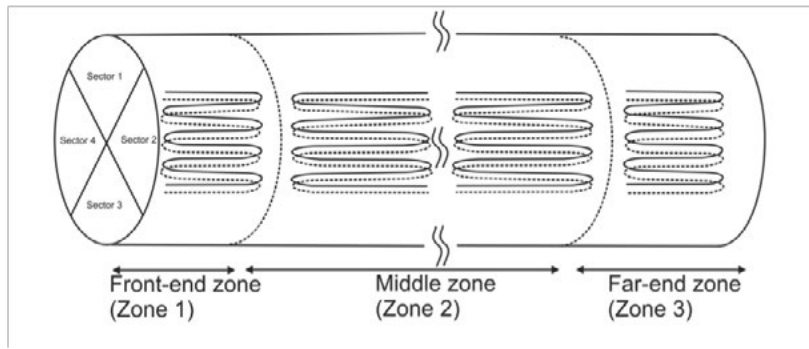


Figure 2-2: The heater layout is divided into three longitudinal zones or sections (front-end, middle and far-end) and into four sectors. In this Figure, only the heater cables in sector 2 are shown.

The secondary heater was installed in the PRACLAY gallery in February 2012. This consists of four heater elements, which were inserted into the central tube inside the part of the PRACLAY gallery that is being heated. The central tube contains five guide tubes (four for heater cables and one for other purposes; see Figure 2-3) and remains accessible at all times so that the heater elements can be replaced if necessary. The secondary heater will only be used in the event of failure of the primary heater. Whereas the primary heater is regulated to provide a constant temperature during the steady heating phase (80°C at the interface between the gallery lining and the Boom Clay), the secondary heater will provide a constant power output, the value of which will be set at the time of the switch-over.

To prevent any impact of unexpected failure of the secondary heater, a back-up of this system was designed and installed. A tube with four elements was inserted inside the central tube (Figure 2-3). The installation of this secondary heater was completed at the beginning of December 2014.

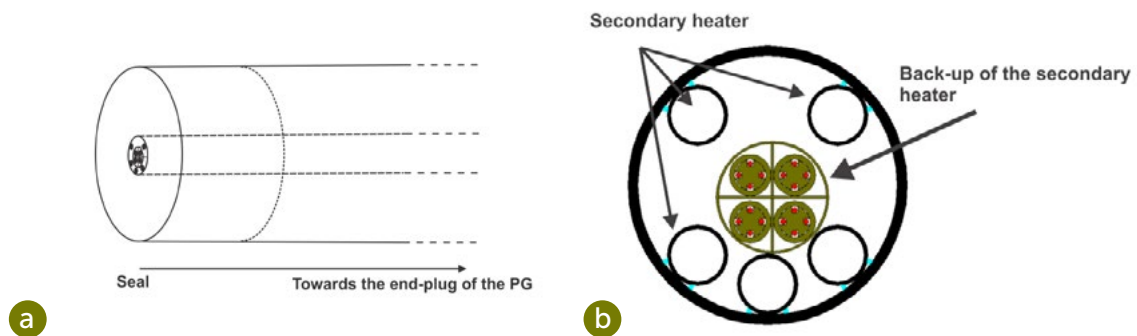


Figure 2-3: Schematic representation of the secondary heating system inside the PG. (a) The secondary heater is located in a central tube. (b) View of the different components inside the central tube defining the secondary heater and its back-up system.

On 3 November 2014, the primary heating system was switched on with a heating power of 250 W/m. On 7 January 2015, a second step was attained and the heating power was increased to 350 W/m. Finally, on 3 March 2015, the heating power was increased to 450 W/m and the heating system was left at this power to reach the target temperature of 80°C at the Boom Clay/concrete lining interface.

	Zone 1 Front-end Zone	Zone 2 Middle Zone	Zone 3 Far-end Zone
Axial length in m	2.26	28.48	3.29
Linear power (3 Nov 2014) in W/m	250 (141 W/sector)	250 (1780 W/sector)	250 (206 W/sector)
Linear power (7 Jan 2015) in W/m	350 (198 W/sector)	350 (2492 W/sector)	350 (288 W/sector)
Linear power (3 March 2015) in W/m	450 (255 W/sector)	450 (3204 W/sector)	450 (370 W/sector)

Table 2-1: Summary of the heating settings for the three zones

## 2.2. Hydraulic seal

As described in the report on the design and installation of the PRACLAY In-situ Experiment (Van Marcke et al., 2013), the seal has to hydraulically cut off the heated part of the PRACLAY gallery from the non-heated part (Figure 2-4). This is achieved by physically closing off the heated part of the gallery and by lowering the hydraulic conductivity of the clay around the seal. To this end, a bentonite ring was installed around a central steel cylinder and in direct contact with the Boom Clay. This bentonite ring has swelled with the absorption of water causing contact with the surrounding clay and allowing the closure of the Boom Clay/bentonite interface. Moreover, a recompression of the Boom Clay was expected due to the swelling of the bentonite, which will locally reduce the effect of the excavation of the gallery (EDZ, excavation-damaged zone).

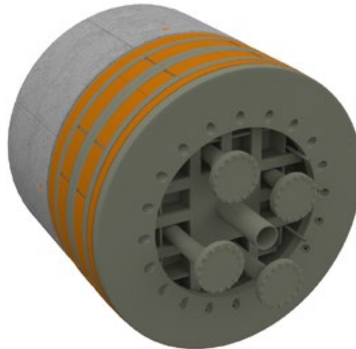


Figure 2-4: 3D view of the seal with a central steel cylinder and an annular ring of bentonite (orange) against the clay.

Because of the importance of this component and because of the high pore water pressure inside the PRACLAY gallery, regular checks are carried out. Since the installation and closure of the seal, the front part of the seal support structure has been regularly cleaned to ensure that even minor leakages, with a potential impact on the pore water pressure in the heated part, can be rapidly detected.

An insulation door (Figure 2-5) was installed on 2 March 2015. An insulated insert (not fully airtight) between the seal and the door prevents too much heat loss from the seal. To get a better idea of the temperature field over the seal structure, eight thermocouples have been installed on the outer surface of the structure.



Figure 2-5: Insulation door (metallic frame and window) in front of seal.

### 2.3. Backfill sand

The part of the PRACLAY gallery that is being heated is filled with water-saturated sand in order to:

- efficiently transfer heat from the heating elements to the surrounding clay;
- create “undrained” hydraulic boundary conditions at the clay/lining interface.

The sand (Mol M34) was put in place by blowing it in a dry state into the gallery before September 2011. Subsequently, about 43 m<sup>3</sup> of tap water was injected into this part of the gallery between January and May 2012 (Figure 2-6). The backfilled gallery was then saturated and pressurized gradually by the natural hydration process, with water from the Boom Clay. The pore water pressure in the gallery has gradually increased since then. On 3 November 2014 it reached 1 MPa, and the PRACLAY gallery was estimated to be fully saturated.

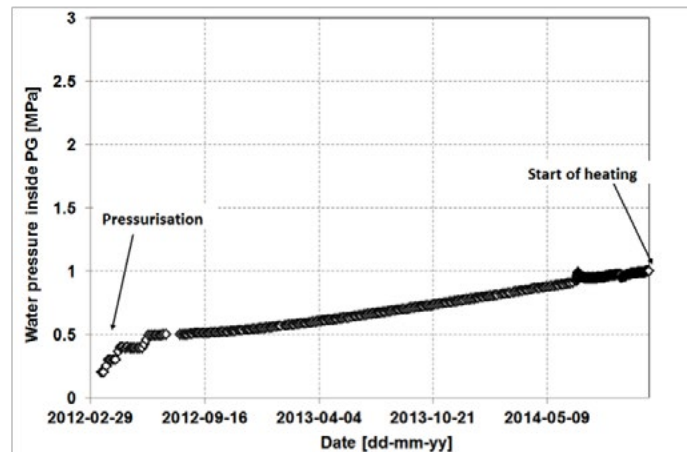


Figure 2-6: Evolution of the pore water pressure inside the backfilled part of PG before switch-on of the heater.

During the heating phase of the experiment, the pressure evolves freely without any human intervention (adding or subtracting an amount of water).

### 2.4. Instrumentation and monitoring system

This section provides a general overview of the instrumentation programme. The PRACLAY In-Situ Experiment has been intensively instrumented with about 1,000 sensors, as shown in Table 2-2 (piezometers, thermocouples, flat-jacks, strain gauges, etc.).

Measurements	Boom Clay	Concrete lining	Seal
Pore water pressure transmitters (piezometer filters)	187	14	21
Temperature (thermocouples)	196	144	46
Total pressure (flat-jacks and Kulite transducers)	28	21	21
Strain gauge (vibrating strain wires)	-	176	-
Topographic survey (total station with prisms)	-	43	5
Displacements (inclinometer/fibre optics)	21	23	2
Relative humidity sensors	-	3	11

Table 2-2: Inventory of the different sensors involved in the PRACLAY experiment

Instrumented boreholes were made from both the Connecting gallery (CG) and the PRACLAY gallery (PG) (Figure 2-7, Figure 2-8 and Figure 2-9). Most boreholes are so-called multi-filter piezometers, which, in addition to the piezometer filters to monitor pore water pressures, also contain thermocouples (same position as the filters) and, optionally, total pressure sensors (flat-jacks or biaxial stress meters) at the deep end of the instrumented casing. Some boreholes were also drilled for displacement measurements (inclinometer and borehole extensometers). In total, the instrumented boreholes contain about 400 sensors around the PRACLAY gallery.

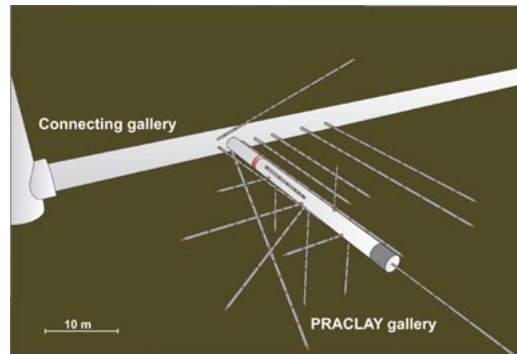


Figure 2-7: 3D view of the instrumented boreholes surrounding the PRACLAY gallery

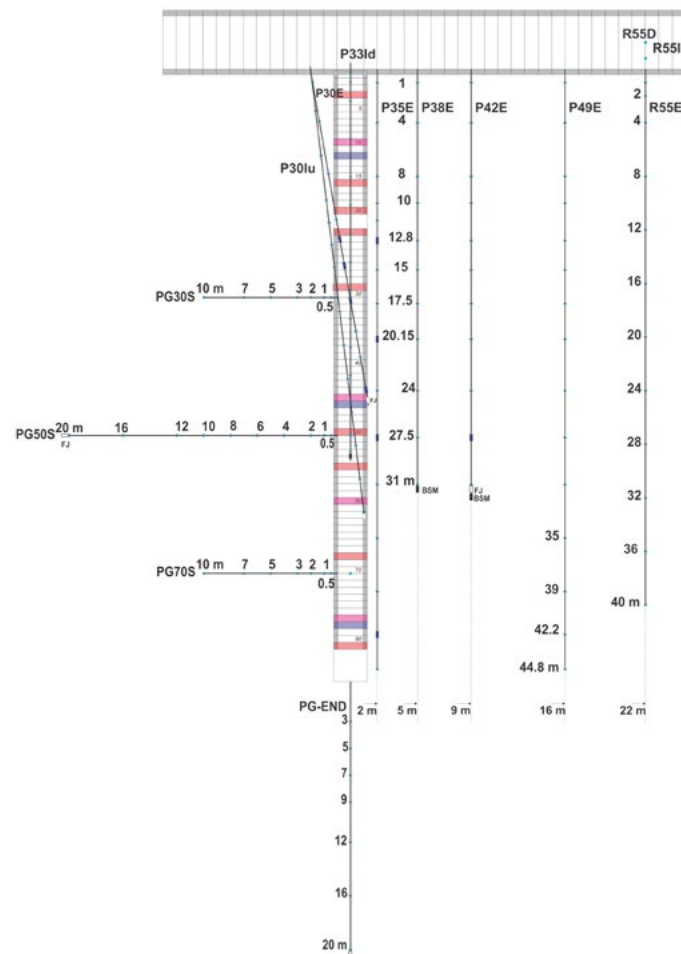


Figure 2-8: Plan view of the PRACLAY gallery, and of the PG and CG boreholes. Coloured rings are instrumented. Dots in the boreholes indicate pore water filters and temperature sensors. The distance from a sensor to the intrados (inner surface) of a gallery (PG or CG) is written beside the sensor.

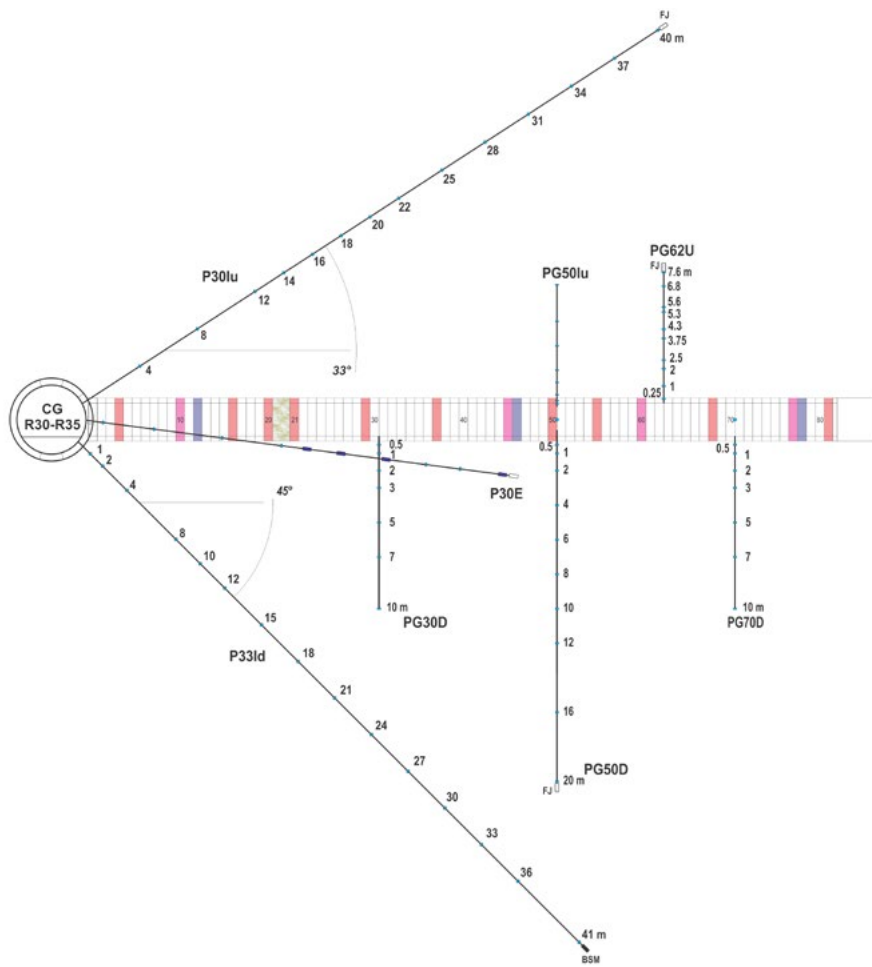


Figure 2-9: Vertical cross-section of the boreholes around the PRACLAY gallery. The distance from a sensor to the intrados of a gallery (PG or CG) is written beside the sensor.

Several segmental concrete lining rings of the PRACLAY gallery have been constructed with instrumented segments (coloured in Figure 2-8 and Figure 2-9) to monitor external radial total pressure on the ring, the normal stresses between the segments (circumferential or hoop stress), the strains and the temperature inside the segments. Moreover, the pore water pressure is measured at different locations inside the gallery. Many thermocouples also monitor the heater cable temperatures. More than 400 sensors have been installed in the gallery and in its lining.

In this report, Ring 50 is referred to as "R50" or "PG50". In the case of a borehole drilled from Ring 50, one or two additional letters are used to indicate the orientation of the borehole. PG50S, for example, is a horizontal borehole from Ring 50 bearing south (D=Down; U=Up; Id=Inclined down; lu=Inclined up).

The instrumentation of the PRACLAY seal is mainly clustered in three zones (sections A, B and C): one located at the upper level ("section A"), one on the right ("section B"), and one on the bottom left ("section C"). Each zone contains total pressure sensors (flat-jacks and piezoresistive types), piezometer filters and thermocouples. The sensors are spread on the radial range from the inner steel cylinder up to the Boom Clay/bentonite interface. In addition, thermocouples have also been installed on the accessible side of the closing plate of the seal. An automated total station, located at the crossing between the Connecting and PRACLAY galleries, is also monitoring the movement of the Seal structure. The Seal instrumentation contains more than 100 sensors.

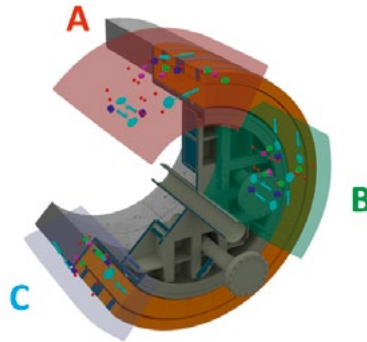


Figure 2-10: Instrumented sections of the Seal, with total pressure sensors (turquoise and green), piezometer filters (blue) and thermocouples (red).

Within the complete instrumentation programme of the PRACLAY In-Situ Experiment, the following measurements are carried out:

#### **Pore water pressure**

Pore water pressures are measured through piezometer filters, incorporated into the instrumented bore-hole casing or embedded inside the gallery backfill or in the bentonite ring of the seal structure. Overall, the pore water pressure is monitored using approximately 220 sensors.

#### **Total pressure**

Total pressure is measured by embedded sensors in different components throughout the experimental set-up. The majority of these sensors are based on flat-jacks. The main applications of these sensors are monitoring the total stress inside the clay formation, at the end of some instrumented boreholes ("FJ" in Figure 2-8 and Figure 2-9). It is also used at the different interfaces of the seal structure, i.e. Boom Clay/bentonite interface, Bentonite/steel central cylinder of the seal and bentonite/downstream flange of the seal. Flat-jacks can also be found at the Boom Clay/concrete lining ring interface and between the concrete segments to estimate the circumferential (or hoop) stress.

Another type of total pressure sensor corresponds to a piezoresistive type (Kulite brand), which is installed in the seal, where flat-jacks were not a suitable solution due to their bigger size.

#### **Temperature**

Temperature is one of the principal parameters of the experiment; hence the set-up is heavily instrumented throughout, mainly with thermocouples because of their robustness. Temperature is measured in the seal, in the concrete segments (intrados, middle and extrados) and in the clay. Instrumented boreholes from the PRACLAY and Connecting galleries are also equipped with thermocouples. In addition, the heater control system uses thermocouples to adjust the power output of the system at any given moment. More than 380 thermocouples have been installed.

### Strain

The most commonly used type of strain gauge is the vibrating wire strain gauge, 176 of which are embedded in the concrete lining segment of four instrumented rings. These are oriented in the circumferential direction of the ring, allowing monitoring of the deformation caused by the loads acting on the concrete segments. Unfortunately, due to an unexpected event, most of the strain gauges failed before reaching 80°C for reasons that are unknown at this time.

### Relative humidity

The accessible part of the gallery is equipped with three sensors to monitor the relative humidity of the air. Originally, several filters inside the seal were also equipped with these sensors, but they stopped working soon after the artificial hydration of the bentonite ring started.

### Displacement

The major set-up for displacement monitoring is based on an automated total station, which is positioned in the gallery crossing, and which measures several times a day the position of the seal structure (visible part) and of several rings of the accessible part of the PRACLAY gallery – in particular to check whether the PRACLAY gallery moves towards the Connecting gallery due to thermal expansion or other (e.g. mechanical) causes.

## 2.5. Data Acquisition system

A basic representation of the data flow process from sensor to data report is shown in Figure 2-11. First, the signal output of the sensors is read and converted into a digital signal by a data logger or a data acquisition front-end. In the PRACLAY experiment, more than 30 data loggers and data acquisition front-ends of different types are used. As a second step, the data acquisition PC controls all these devices and converts the different data formats into one standard format that can be read by the server. Another important functionality of the data server is that it performs the data conversions, i.e. calculating engineered data from raw data.

For the follow-up of the experiment, visualisation software that accesses the data from the server is used.



Figure 2-11: Schematic representation of the data flow. From left to right: sensor, data logger, data acquisition PC, database server and visualisation software.

A selected set of sensors is checked automatically by the database server, looking for deviating measurements. If alarms limits are exceeded, e-mail notification is sent. In addition to these database alarms, hardwired alarms have been implemented for the most critical parameters, such as pore water pressure in the gallery and heater parameters. Some operational components of the experimental set-up, such as the heater control system and the power supplies, are also connected to a hardwired alarm system. This hardwired alarm system functions independently of the data acquisition system for maximum reliability.

### 3. Test evolution

This section describes the main results since the switch-on of the heating system on 3 November 2014 until the target temperature of 80°C was reached at the interface of the Boom Clay and the concrete lining.

The power of the heating system was increased stepwise to reach the target temperature of 80°C at the Boom Clay/lining interface. The heater was switched on on 3 November 2014 with a constant power of 250 W/m for the three zones of the primary heating system. Two months later (on 7 January 2015), the power was increased from 250 W/m to 350 W/m. On 3 March, the power was again increased to 450 W/m and maintained until the temperature at the extrados of the concrete lining segment reached 80°C (19 August 2015). Table 3-1 summarises the history of the applied heating power during the start-up phase.

	Zone 1 Front-end Zone	Zone 2 Middle Zone	Zone 3 Far-end Zone
Axial length in m	2.26	28.48	3.29
Linear power (3 Nov 2014) in W/m	250	250	250
Linear power (7 Jan 2015) in W/m	350	350	350
Linear power (3 March 2015) in W/m	450	450	450

Table 3-1: shows the measured heating power in one of the heater zones during this start-up phase.

Figure 3-1 shows the measured heating power in one of the heater zones during this start-up phase.

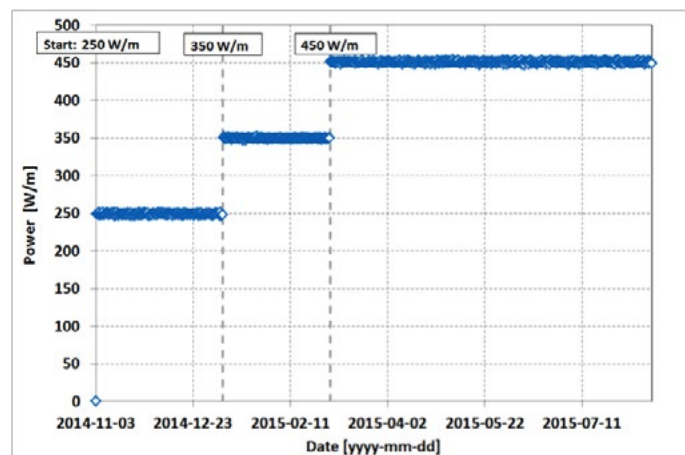


Figure 3-1: Evolution of the measured heating power in W/m.

This section will first present the observations of the so-called “test-control parameters”, i.e. the temperature in the concrete lining (intrados and middle), the temperature at the Boom Clay/concrete lining (extrados) interface and the pore water pressure inside the backfilled part of the gallery. These three parameters are the main parameters controlling the THM boundary conditions of the experiment.

The response inside the Boom Clay is presented with a focus on Ring 50 of the PRACLAY gallery in the middle of the heated section, followed by comparison with the other boreholes from the PRACLAY gallery and comparison with the observations from boreholes from the CG.

Finally, the different responses in the bentonite seal (total stress, pore water pressure and temperature) and within the concrete lining rings (stress) are presented.

### 3.1. Temperature in the concrete lining and at the lining/Boom Clay interface

Once the power was switched on, the temperature started to increase in the concrete lining rings. In order to track the temperature evolution inside the concrete segments of the gallery, thermocouples were embedded in 10 concrete lining rings of the gallery, as shown in Figure 3-2.

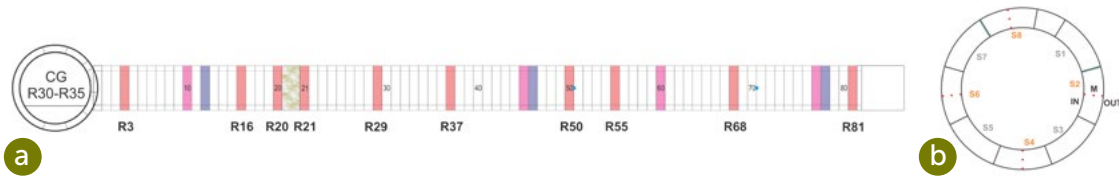


Figure 3-2: (a) View of the 10 lining rings of the PG instrumented with thermocouples (R3, R16, R20, R21, R29, R37, R50, R55, R68, R81). (b) Position of the temperature sensors inside the instrumented segments (S2, S4, S6 and S8; IN: inner, M: middle and OUT: outer).

Figure 3-3 shows the temperature evolution inside Ring 50 (PG50), located in the middle of the heated part of the PG (Figure 3-2). The temperature in the different segments increases in a similar way except for segment 2 (slower increase). The different power steps of increase can be observed, with a rapid temperature increase at each new step, followed by a decrease in the temperature increase rate with time. At the end of the start-up phase (August 2015), the temperature at the extrados is about 80°C while at the intrados, a value close to 85°C is obtained. This means that the temperature difference over a segment is approximately 5°C.

The temperature in segment S2 evolves more slowly than in the other rings. This difference is explained by the presence of an open borehole at this specific position in the gallery lining. This behaviour will be explained and highlighted during the description of the results in the different boreholes around PG50.

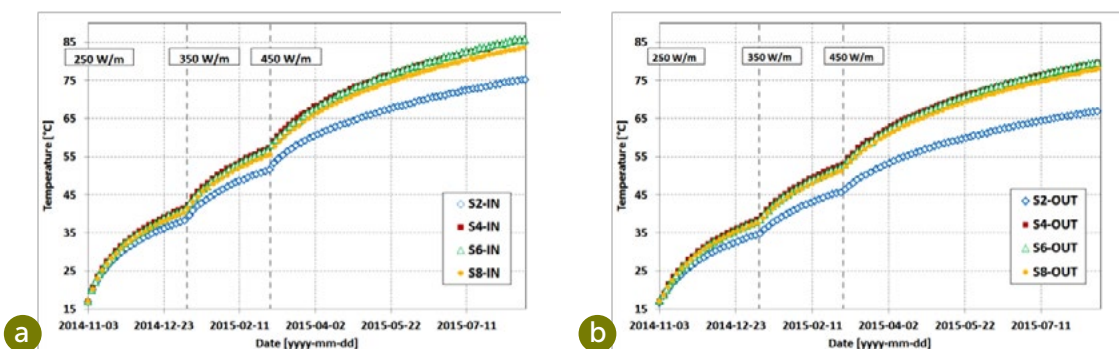


Figure 3-3: Temperature evolution in four segments of Ring 50 (IN: inner or intrados, OUT: outer or extrados).

Figure 3-4 shows the longitudinal profiles of the lining temperature, in the direction parallel to the gallery axis, at different steps of the start-up phase. The temperatures are measured at the outer surface of the S6 segments (left side of the PG) of the different instrumented lining rings. The profiles show a rather uniform temperature increase along the heated part of the PRACLAY gallery at the beginning of the experiment. At the end of the start-up phase, however, a temperature gradient is observed. The temperature decreases along the gallery from R37 ( $\approx 19$  m) to R81 ( $\approx 40$  m).

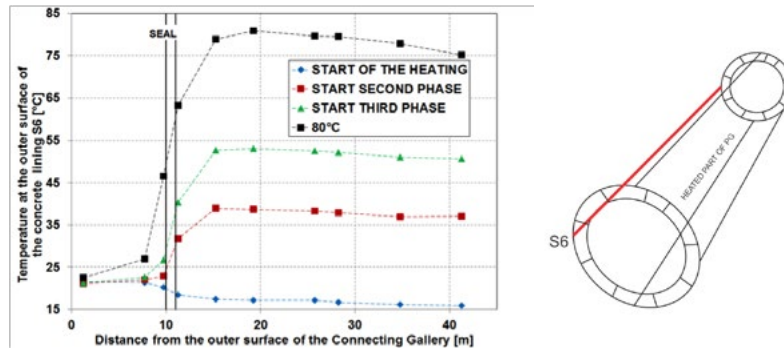


Figure 3-4: Evolution of the extrados temperature profiles along the heated part of the PRACLAY gallery (measured on the outer surface of the “S6” segments of the different instrumented lining rings).

Similar longitudinal temperature profiles are observed in the other segments when 80°C is reached, as can be seen in Figure 3-5. The temperature evolution is generally homogeneous between the different positions (S4, S6, S8). However, Figure 3-5 shows a lower measured value for S2, at the position of Ring 50, due to the presence of the open borehole PG50S. All the longitudinal profiles show the same decrease in temperature from Ring 37 to Ring 81. Nevertheless, it is observed that the temperature close to the seal structure is higher at the top of the gallery (S8) compared with the other segments (S2, S4, S6). For now, there are no reasonable explanations for this last observation. The top segments (S8) register higher temperatures in the non-heated part of the PRACLAY gallery. This can be explained by the presence of lights at this position, which increase the temperature of the concrete locally.

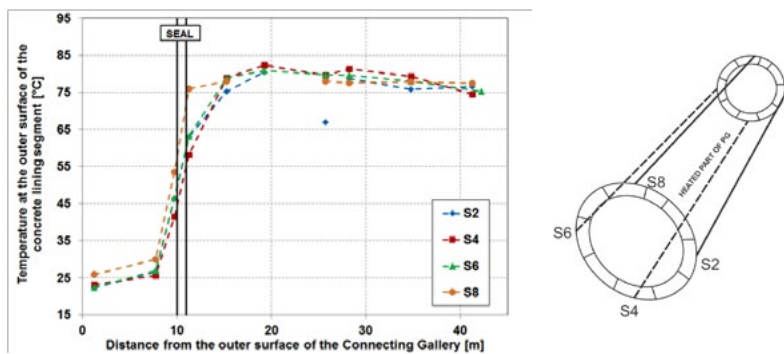


Figure 3-5: Temperature profiles along the outer surface of the concrete lining segment at different locations in the gallery at the end of the start-up phase (80°C).

Figure 3-6 shows the longitudinal profiles of temperature along the three positions inside the concrete lining for S2 at the end of the start-up phase. A fairly uniform temperature gradient between the inner and the outer surface is obtained along the gallery. The measured temperatures at the specific location of PG50 show the effect of the open borehole across the lining.

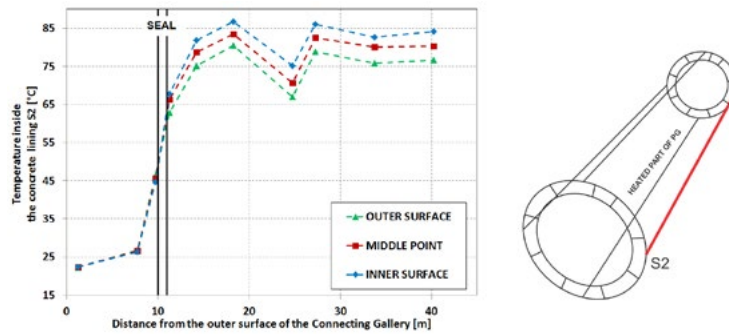


Figure 3-6: Temperature profiles along the outer and inner surfaces of the south side of the gallery and at mid-thickness of the lining at the end of the start-up phase (measured on the S2 segments of the different instrumented lining rings).

The previous two graphs show that the longitudinal temperature profiles display some variations between the different segments. More particularly, the temperature measured close to the seal in segment S8 is higher than at the other ring segments. Moreover, a slight temperature gradient from the seal to the far end of the gallery is observed. Indeed, Figure 3-5 shows a temperature of around 80°C at a distance of approximately 19 m, while at the far end of the gallery, the temperature reaches a value of around 75°C.

Because of these slight variations in temperature, an indicator for the target temperature of 80°C has been defined as the average temperature over the reliable thermocouples at the outer surface of Rings 37, 50 and 55 (the temperature at the outer surface of S2 in Ring 50 is not included because of its non-representativeness, as explained previously). Figure 3-7 shows the evolution of this average temperature. The different heating phases are clearly visible on this graph. It can also be seen that 80°C was reached in mid-August 2015.

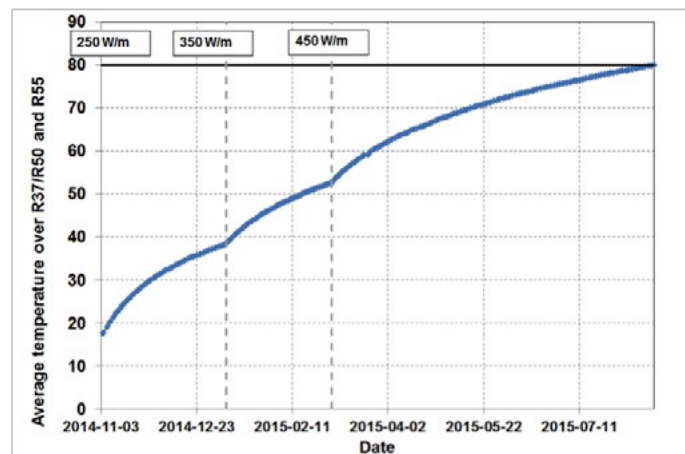


Figure 3-7: Average temperature evolution over the three rings (R37/R50/R55). The average temperature is calculated using the measurements from the thermocouples at the extrados of the lining.

### 3.2. Backfill pore water pressure

A number of filters are installed inside the backfilled part of the gallery with the goal of monitoring the pore water pressure inside. As already explained, this backfilled part was pressurised by injecting water before the start of the heating phase. Once the pressure reached 0.5 MPa, it was left to evolve without any additional injection of water. Because of Boom Clay water inflow, the pressure rose to a value of

around 1 MPa just before the start of heating.

Heating generates an excess pore water pressure inside the gallery due to a higher thermal dilation coefficient of water compared with the solid phase (sand, concrete). The evolution of the pressure inside the backfilled part of the PRACLAY gallery can be seen in Figure 3-8. It is observed that the effect of heating was instantaneous. This confirmed an initial water saturation of the system. The different heating steps can be clearly seen in this Figure. A value of 2.9 MPa was reached when the temperature measured 80°C at the extrados of the concrete lining.

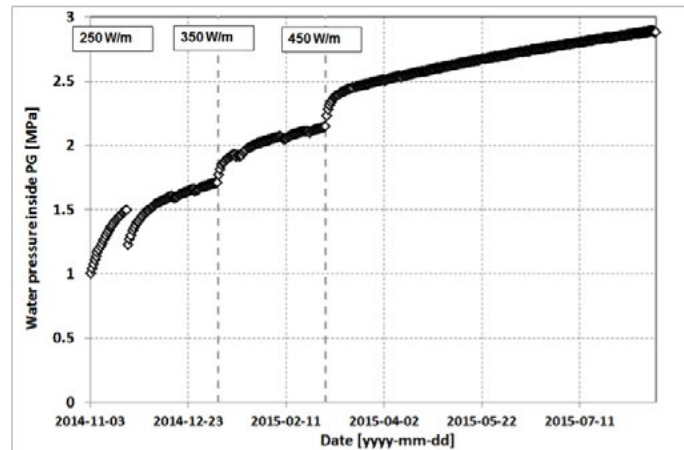


Figure 3-8: Pore water pressure inside the PG.

A sudden drop in pressure (from 1.5 to 1.0 MPa) was observed on 22 November 2014. After 11 days and without any intervention, the pressure recovered to its initial value before the drop. This pressure drop might be due to a rearrangement of the experimental set-up (concrete lining, older boreholes, etc.), which had never been pressurised up to this level before. Following this pressure drop, a general decrease in pore water pressure was observed around the gallery and in the clay a short distance from the extrados. Besides this sudden large pressure drop, some small variations were observed during the first months of 2015. These were caused by small leakages of the fibre optics installed in the PG passing through the seal. To avoid further leakages, the fibre optics were disconnected and sealed.

### 3.3. Boom Clay responses

#### 3.3.1. Observations around Ring 50 of the PRACLAY gallery

The response of the Boom Clay to heating is mainly monitored through the instrumented boreholes drilled either from the PRACLAY gallery or from the Connecting gallery, as shown in Figure 3-9 and Figure 3-10, in which the distance of each sensor (piezometers and thermocouples) from its corresponding gallery lining intrados is indicated. The distance of the Connecting gallery boreholes from the axis of the PRACLAY gallery is also shown. The focus is on Ring 50. Because of the central position of this ring, these boreholes are considered to be the most representative for the experiment.

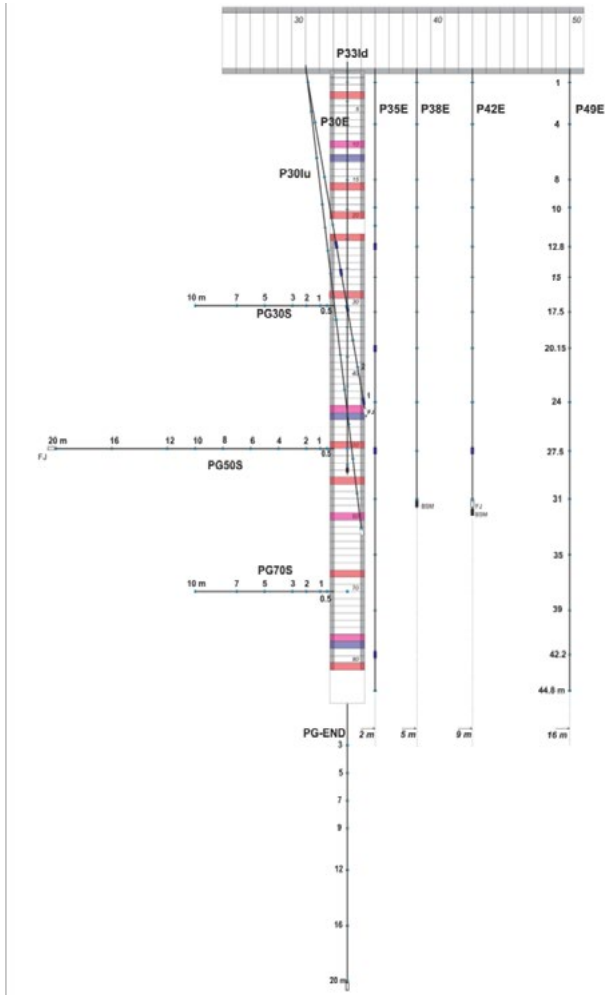


Figure 3-9: Presentation of the instrumentation around the PG, including the borehole drilled from the CG. This diagram corresponds to a horizontal cross-section taken in the middle of the axis of PG.

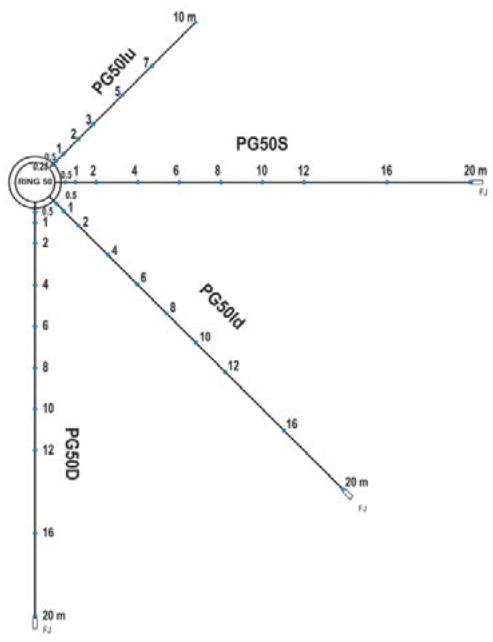


Figure 3-10: Vertical cross-section of the different boreholes at Ring 50 of the PG. The orientation of a borehole is indicated by one or two letters (S=south (horizontal); D=down; ld=Inclined down; lu=Inclined up). The number refers to the distance of the sensors from the intrados of the gallery lining.

### Temperature evolution

Figure 3-11 shows the temperature evolution as measured by four sensors located along the horizontally instrumented borehole PG50S (drilled from R50). At the end of the start-up heating phase (August 2015), the heated zone extended over approximately 10 m. At the sensor closest to the PG, at a distance of 0.5 m from the intrados, the temperature reached approximately 47°C.

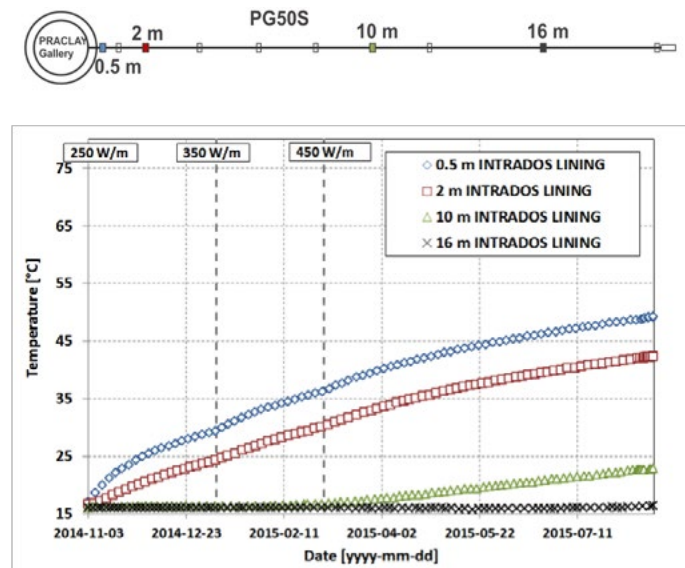


Figure 3-11: Temperature evolution for some selected sensors installed in borehole PG50S.

Figure 3-12 shows the temperature evolution in borehole PG50D, drilled vertically from Ring 50 in the PRACLAY gallery, as can also be seen in Figure 3-10. The different heating phases can be observed. At the end of the reporting period, the temperature in the sensor closest to the PRACLAY gallery, at a distance of 0.5 m from the inner surface, is almost equal to 67°C. The affected temperature zone is less than 10 m for this borehole.

Comparing with the observations from PG50S, it is noted that the affected thermal zone is smaller and that a higher temperature with a higher temperature gradient is reached for borehole PG50D. These differences can be partly explained by the fact that the boreholes were left open with the water free to move. As a consequence, a convection cell could be generated in the horizontal and upward boreholes, locally enhancing heat transfer through these boreholes. The downward borehole does not show this artefact because, in this case, the hot water is located at the top of the borehole close to the PG, while the cold water is at the bottom of it. So the mechanism of natural convection cannot take place in this last case.

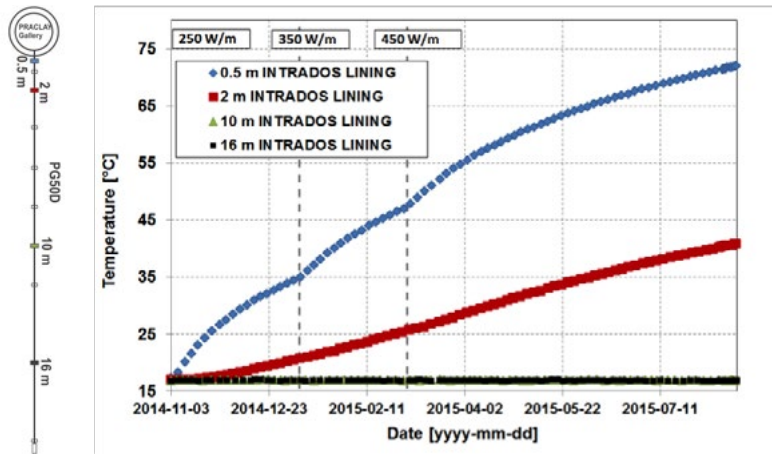


Figure 3-12: Temperature evolution in selected thermocouples installed in borehole PG50D.

### Pore water pressure evolution

Figure 3-13 and Figure 3-14 show the evolution of the pore water pressure around Ring 50 measured from the horizontal (PG50S) and the vertical (PG50D) boreholes, respectively. The initial state of the pore water pressure prior to heating depends on the effect of drainage of the PG when the gallery was open and on the backfilling and pressurisation of the gallery. Consequently, a pore water pressure gradient is observed around the gallery, as seen in Figure 3-13 and Figure 3-14, at the beginning of the heating phase.

Generally, the pore water pressure increases with the temperature evolution over time. The magnitude of this pressure increase is almost the same in both directions (horizontal and vertical) for filters installed at a comparable distance from the gallery.

The hydraulically affected zones are different for both boreholes. Variations are observed at a distance of up to 10 m for PG50S, while the influence of heating appears to be around 20 m in vertical borehole PG50D. However, the last two sensors of PG50D indicate an unforeseen evolution. As can be seen in Figure 3-14, the pore water pressure of PG50D at a depth of 16 m unexpectedly increases a few weeks after the third heating phase and stabilises before reaching 80°C. This observation is confirmed by the pore water pressure profile in Figure 3-16, which shows unexpected measurements at depths of 16 and 20 m. This behaviour is not yet fully understood and is under investigation. Consequently, the hydraulically affected zone in the vertical direction has to be considered with caution.

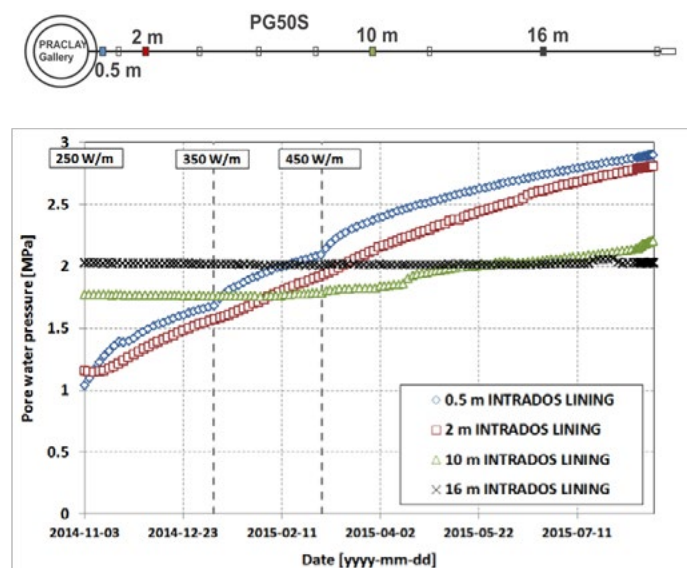


Figure 3-13: Evolution of the pore water pressure in selected piezometers of PG50S.

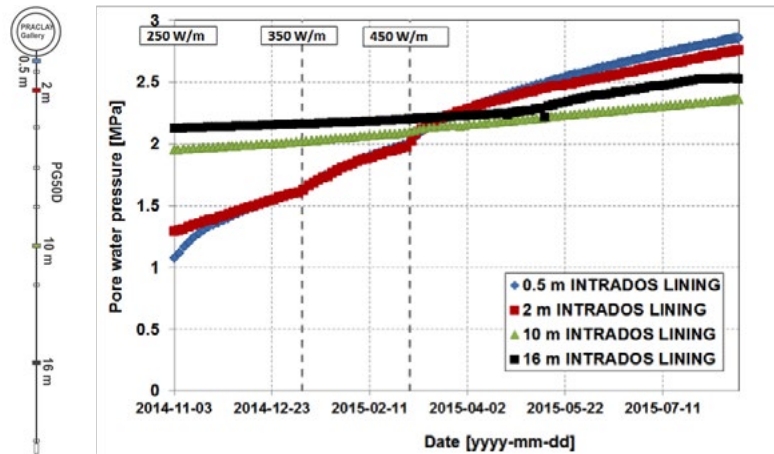


Figure 3-14: Evolution of the pore water pressure in selected piezometers of PG50D.

Figure 3-15(a) presents a comparison between two filters at a distance of 2 m from the intrados of the PRACLAY gallery in PG50D and PG50S, respectively. During the first two heating steps, the evolution of pore water pressure was almost the same, whereas during the third, a higher dissipation of pore water pressure is observed for the vertical piezometers. This might be explained by a likely higher hydraulic conductivity in the horizontal direction. At the beginning of the first heating step, the pore water pressure in the sensor in the horizontal borehole shows an initial slight decrease before increasing (Figure 3-15(b)). This phenomenon is similar to observations made during the small-scale in-situ ATLAS experiment (Chen et al., 2011). However, unlike the ATLAS experiment, it was only observed at the beginning of the first heating step of the PRACLAY experiment and not at each heating step.

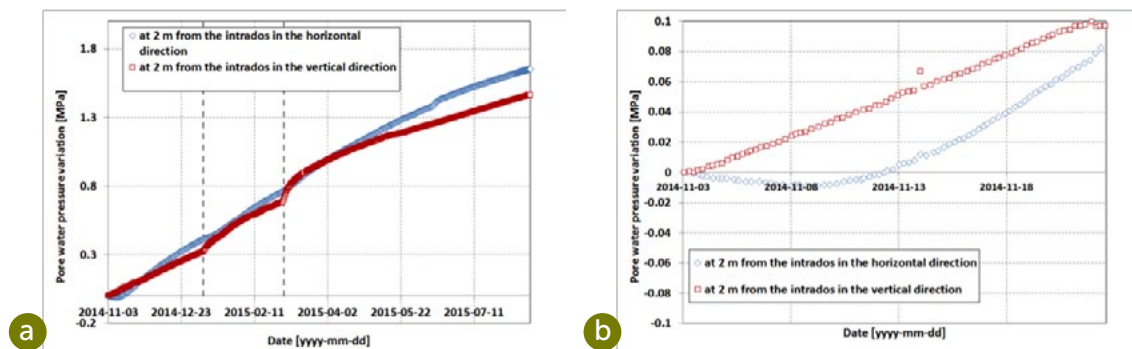


Figure 3-15: (a) Pore water pressure evolutions of filters 8, at a distance of 2 m from the intrados of PG50S (horizontal borehole) and PG50D (vertical borehole). (b) Zoom of the pore water pressure variation around the start of the heating phase.

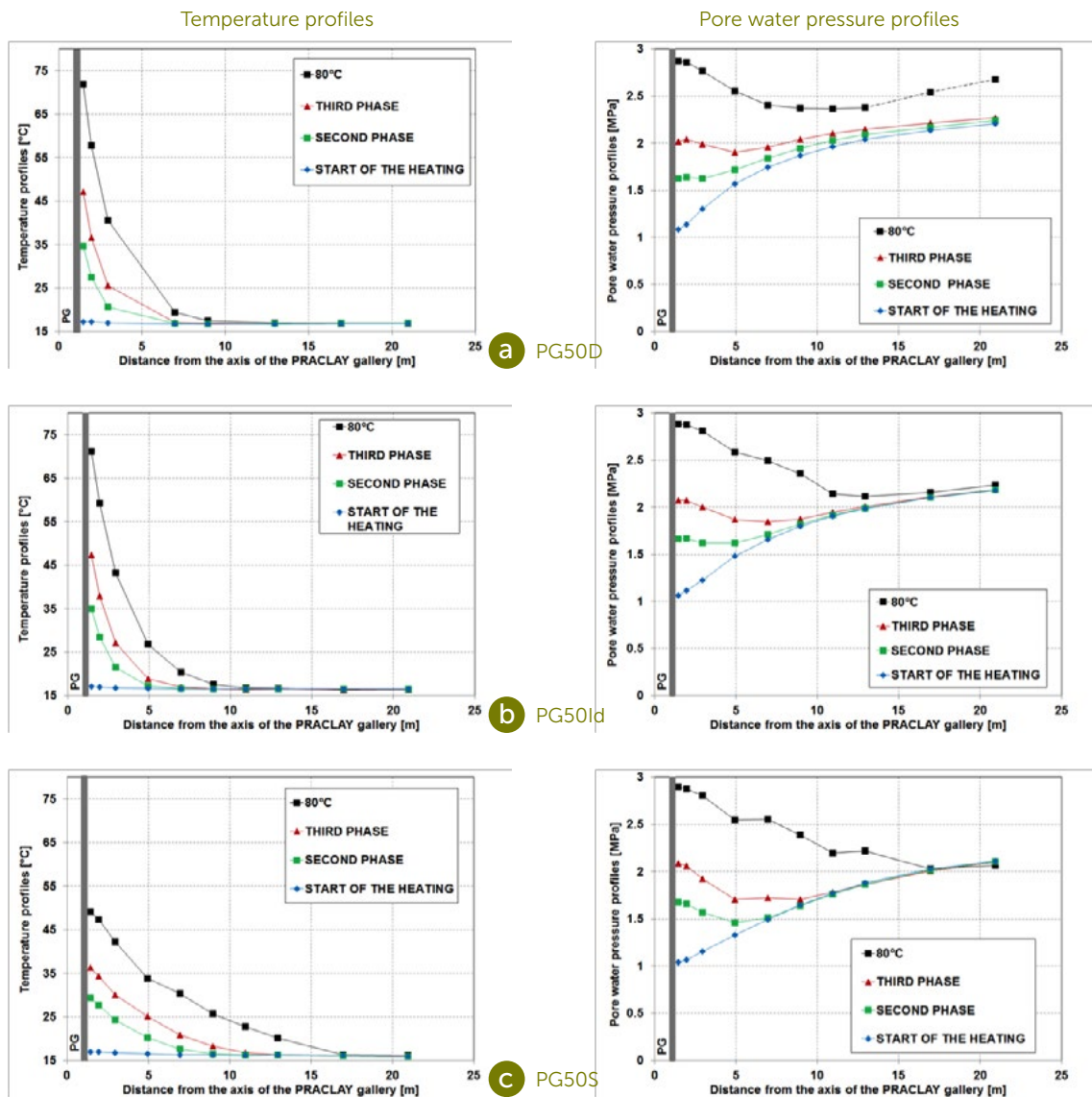
### Temperature and pore water pressure profiles

Four boreholes were drilled from Ring 50 (PG50) in different directions (Figure 3-10 and Figure 2-9) and were instrumented to monitor the pore water pressure, temperature and total pressure in the clay.

Figure 3-16 shows the temperature and pore water pressure profiles for different times for the four boreholes around the PG. A general temperature increase is observed in the clay. This increase differs according to the direction, as seen, for example, in PG50D (Figure 3-16(b)) and PG50S (Figure 3-16(c)). Close to the gallery, when the target temperature of 80°C is reached, the temperature is higher for the downward borehole (70–75°C), while the maximum is lower than 50°C for PG50S and PG50lu (see Figure 3-17(a), which is a comparison of the profiles of the temperature variation for the four boreholes around Ring 50 of the PG). Furthermore, the thermally affected zone is smaller than 10 m in PG50D and PG50Id

compared with PG50S and PG50lu, where it extends further than 10 m. This effect is linked to the open boreholes, which allow the formation of a convection cell inside the casing of the piezometer tube, enhancing heat transfer through the casing.

In terms of pore water pressure, the magnitude of the increase is approximately similar for all of the profiles with a maximum value of around 2.9 MPa when the target temperature of 80°C is reached (Figure 3 17(b), which is a comparison of the profiles of the pore water pressure variation for the four boreholes around Ring 50 of the PG). The hydraulically affected zone is around 15 m for all of the boreholes, with the exception of PG50D. In the latter case, an unexpected modification of the fluid flow seems to take place after the third heating step. The reason for this higher pore water pressure at the end of this borehole is unexplained at the time of reporting and is under investigation.



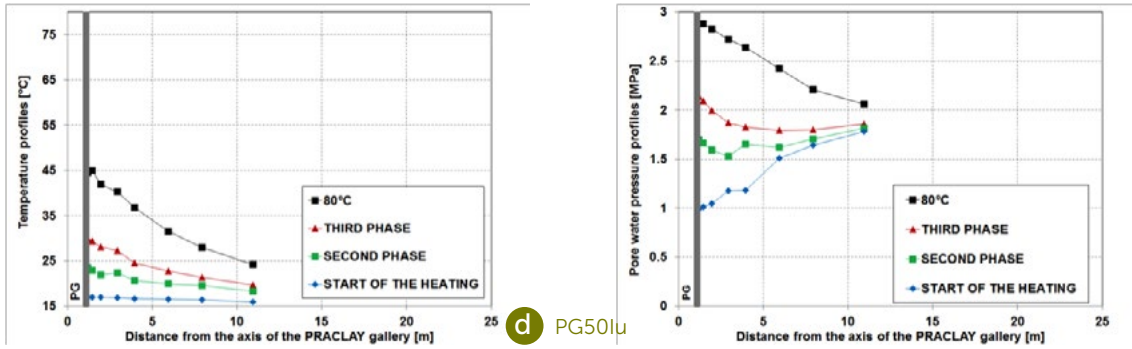


Figure 3-16: Profiles of pore water pressure and temperature for the boreholes around R50.

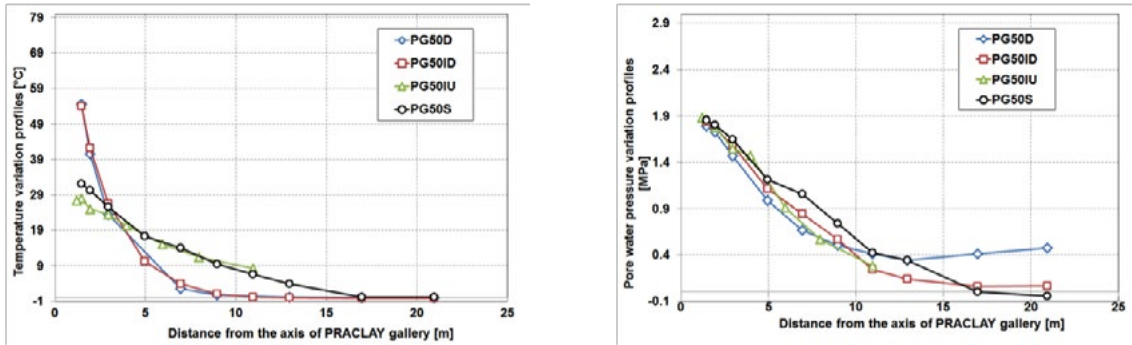


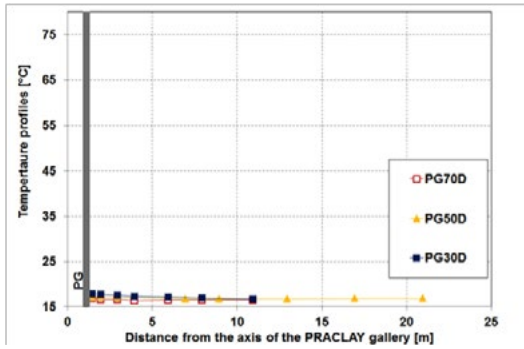
Figure 3-17: Variation in temperature and pore water pressure along different directions around R50 at 80°C

### 3.3.2. Temperature and pore water pressure profiles at other rings along the PRACLAY gallery

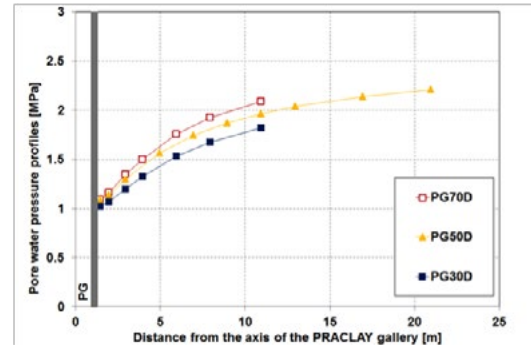
The observations around Ring 50 show that the temperature evolution diverges from one direction to another one. The heat transfer in the horizontal and upward boreholes is assumed to be enhanced. However, the pore water pressure evolution in the clay is consistent for the different directions.

A comparison between the different **vertical boreholes PG30D, PG50D and PG70D** (see Figure 2-8 and Figure 2-9 for their positions) is given in Figure 3-18 for different times. Consistent, homogeneous behaviour is observed for the three boreholes along the axis of the PRACLAY gallery for both temperature and pore water pressure. This means that the thermally and hydraulically affected zones (around 10 m for thermal and up to 15 m for hydraulic) are similar along the PRACLAY gallery axis for at least the distance between PG30 and PG70.

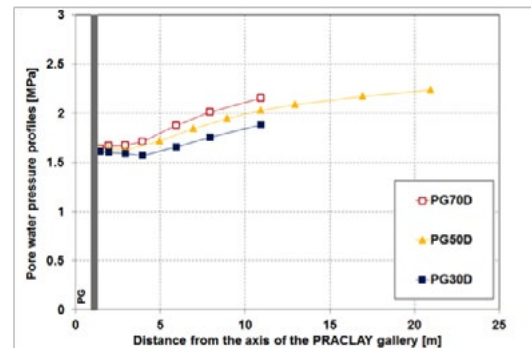
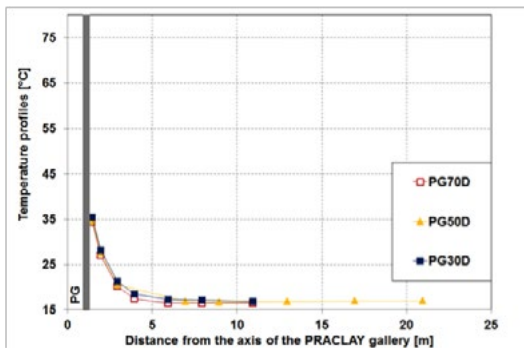
Temperature profiles



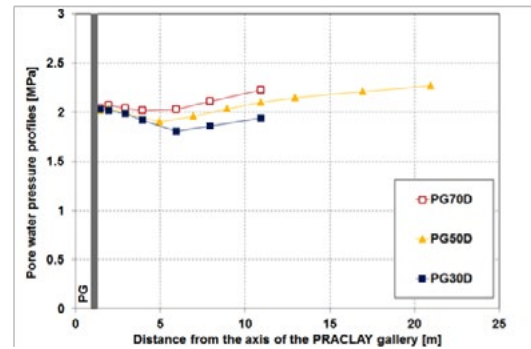
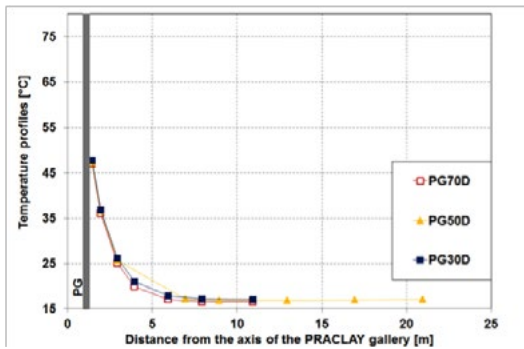
Pore water profiles



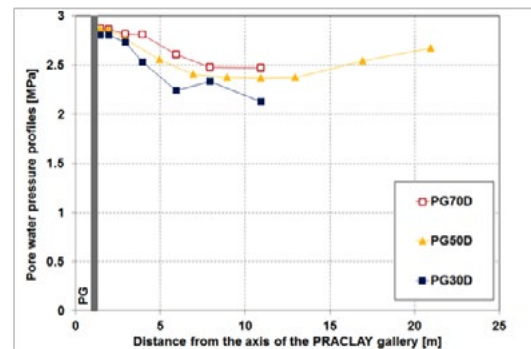
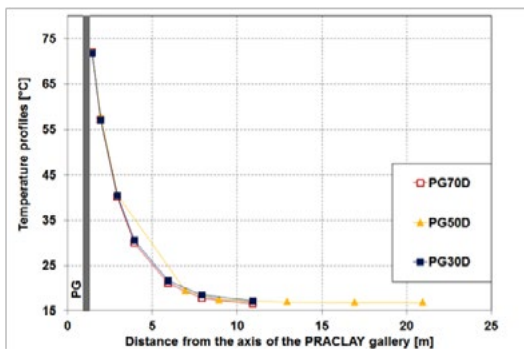
a At the time of the switch-on: 250 W/m



b At the beginning of the second phase: 350 W/m (after 65 days at 250 W/m)



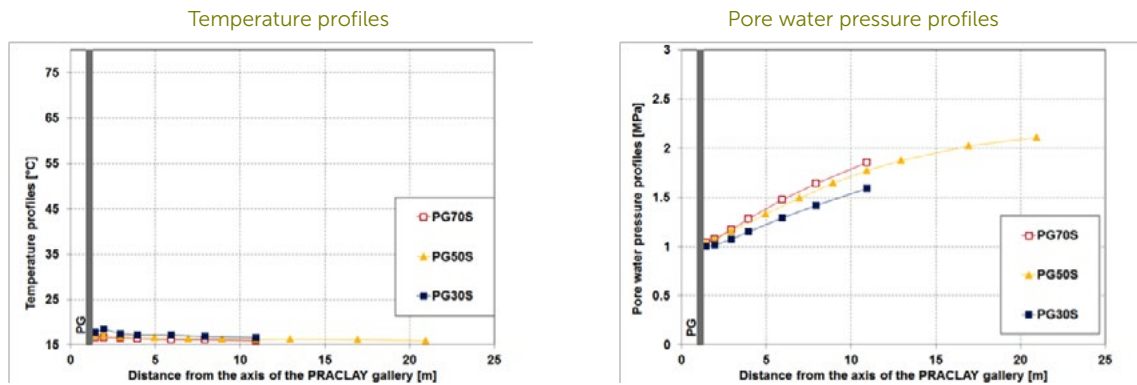
c At the beginning of the third phase: 450 W/m (after 55 days at 350 W/m)



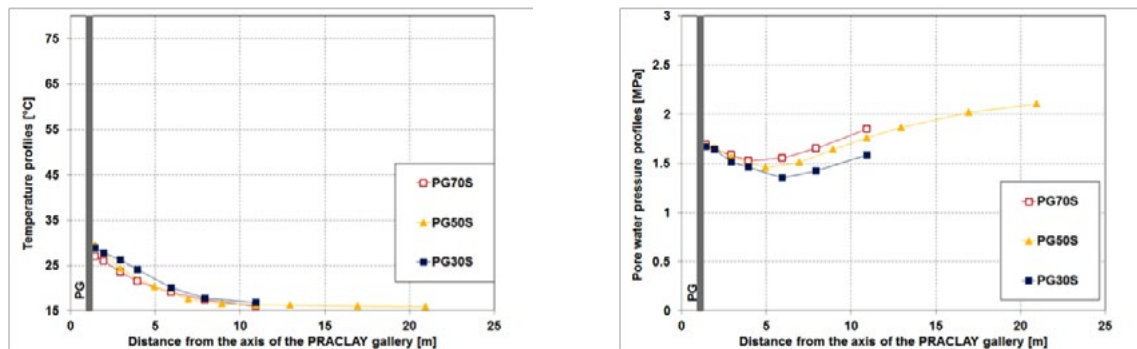
d 80°C (after 169 days at 450 W/m)

Figure 3-18: Pore water pressure and temperature profiles for the three boreholes PG30D, PG50D and PG70D, at different times: start of the experiment, start of the second and third phases and at 80°C.

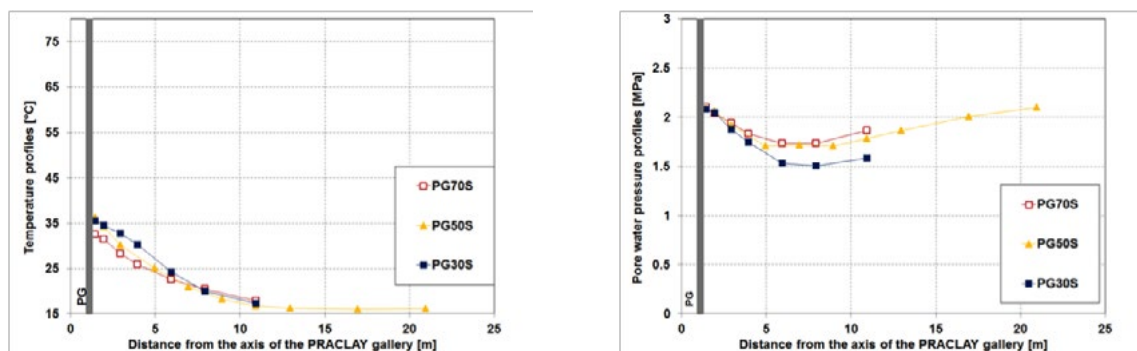
This section discusses the comparison between the **horizontal boreholes** of the PG. Figure 3-19 shows the temperature and pore water pressure profiles for **PG30S, PG50S and PG70S** (see Figure 3-9 for their positions). Again, this comparison is made at different times during the experiment: at the start, at the beginning of the second phase, at the beginning of the third phase and when 80°C is reached. A general observation is that the evolution of the temperature and pore water pressure is consistent between the three different boreholes. The effect of the open boreholes enhancing heat transfer by convection is observed and is confirmed for all three horizontal boreholes, as can be seen in the temperature profiles. Indeed, comparing with the temperature of the downward boreholes (Figure 3-18), the maximum temperature close to the lining depends on the orientation of the boreholes: a maximum temperature of around 50°C is observed for the horizontal direction, while the maximum value is around 70°C for the downward boreholes.



a At the time of the switch-on: 250 W/m



b At the beginning of the second phase: 350 W/m (after 65 days at 250 W/m)



c At the beginning of the third phase: 450 W/m (after 55 days at 350 W/m)

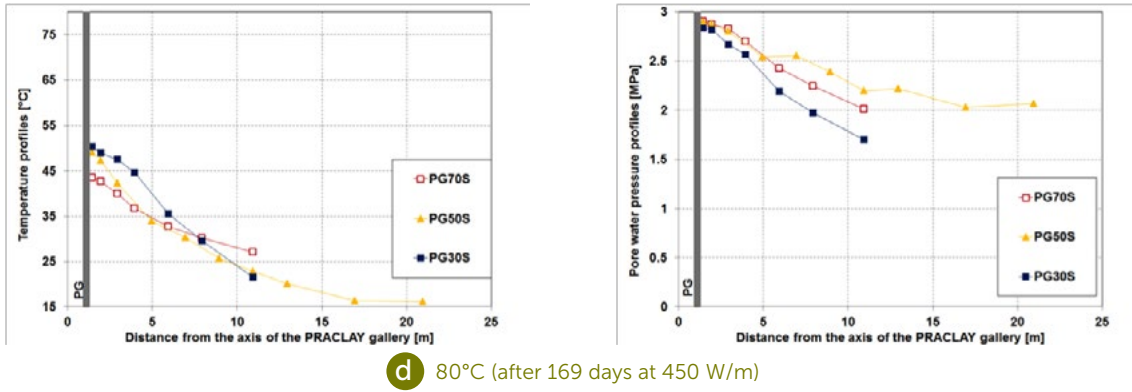


Figure 3-19: Pore water pressure and temperature profiles for the three boreholes PG30S, PG50S and PG70S, at different times: start of the experiment, start of the second and third phases and at 80°C.

### 3.3.3. Temperature and pore water pressure profiles in boreholes drilled from the Connecting gallery

In this section, typical results from the boreholes drilled from the Connecting gallery are presented. Figure 3-20 shows the temperature and pore water pressure evolution for selected sensors in P35E drilled from the Connecting gallery and parallel to the PRACLAY gallery axis (2 m from the axis). The same conclusions can be drawn. An excess pore water pressure caused by an increase in temperature is observed with different magnitudes, depending on the locations of the sensors. The evolution is quite uniform for the sensors close to the heated zone.

For the sensors further from the heated zone, located 10 m and 44.8 m from the intrados of CG, a lower temperature and a lower pore water pressure are observed. This is particularly true for the sensor situated 10 m from the intrados of the Connecting gallery because of the presence of the seal, which acts as an impervious boundary condition and therefore limits the increase in the pore water pressure outside the heated part of the PG.

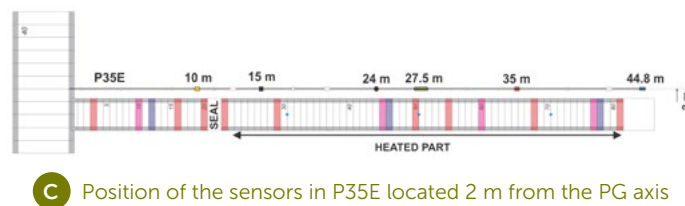
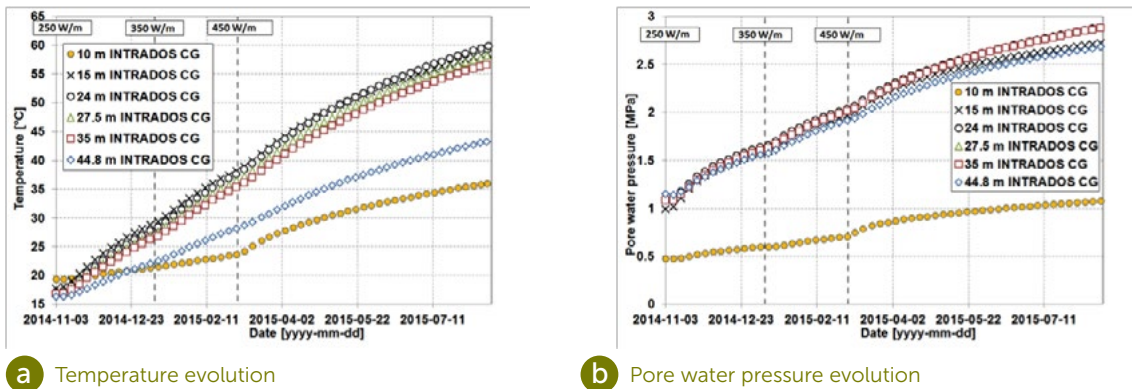


Figure 3-20: Evolution of temperature and pore water pressure in borehole P35E, which is parallel to the PG axis, as can be seen in c).

Figure 3-21 shows the temperature and pore water pressure profiles for P35E. A temperature and pore water pressure increase has been observed since heating began. Both exhibit a relatively uniform evolution along the length of the PG from the seal to the deep end of the PRACLAY gallery. The presence and effect of the hydraulic seal can clearly be seen in these graphs. Nevertheless, a slight decrease in the temperature field with distance from CG is observed. This might be explained by the fact that the last two sensors (located at 42.2 m and 44.8 m) at the end of the profile are slightly outside the heated part of the gallery and that the borehole was drilled prior to the PRACLAY gallery excavation. Displacement of the sensors towards the axis of the PRACLAY gallery due to convergence of the clay during and after excavation cannot be excluded.

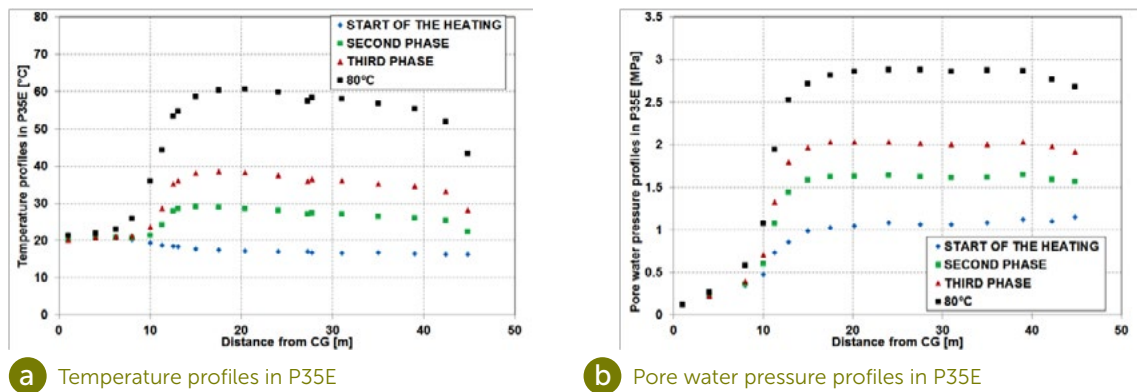
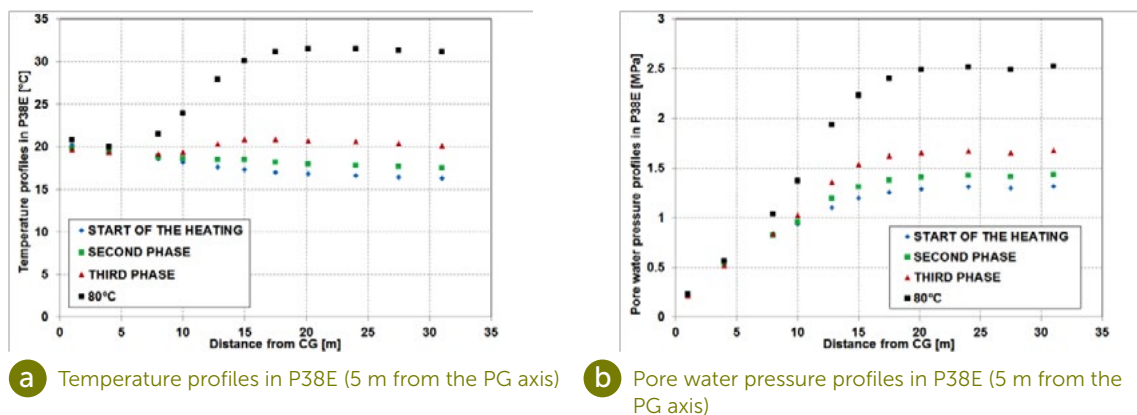
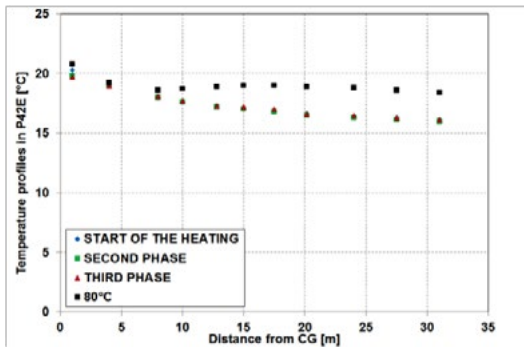


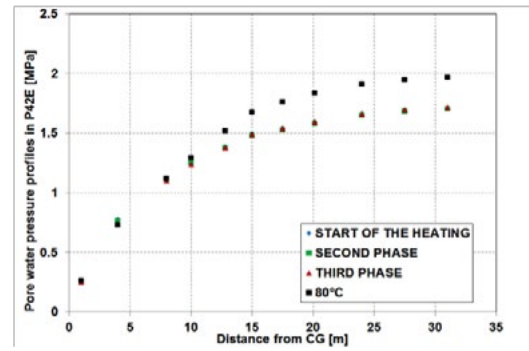
Figure 3-21: Temperature and pore water pressure profiles in P35E

Figure 3-22 shows the temperature and pore water pressure profiles for the three boreholes P38E, P42E and P49E parallel to the axis of the PRACLAY gallery but at different distances from it (see Figure 3-9 for their positions). The same conclusions as previously can be drawn, with the generation of an excess pore water pressure increase caused by the rise in temperature of the clay. The measurements for P38E and P42E clearly show the effect of the hydraulic seal. Conversely, no reactions have yet been seen for P49E, defining the limit of the thermally affected zone, i.e. for both the temperature and the pore water pressure. From this last observation, the size of the hydraulically affected zone can be estimated to be less than 16 m (from the PG axis) in the horizontal direction. The estimation of the extent of the thermally and hydraulically affected zones based on these observations is consistent with that derived from the boreholes that are drilled from the PG.

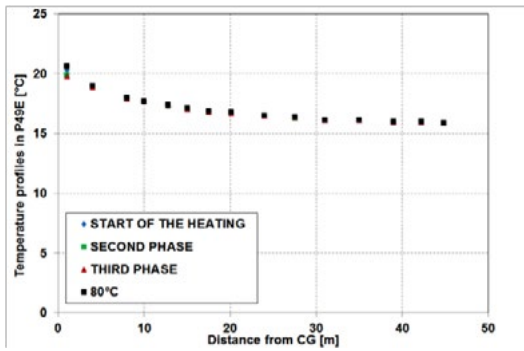




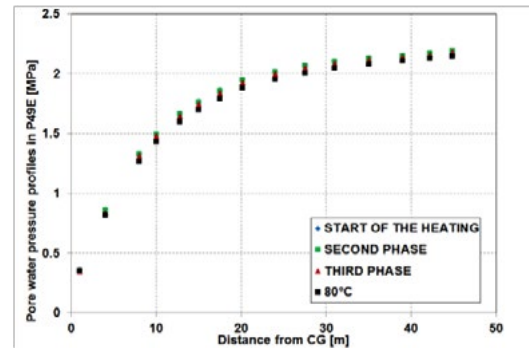
c Temperature profiles in P42E (9 m from the PG axis)



d Pore water pressure profiles in P42E (9 m from the PG axis)



e Temperature profiles in P49E (16 m from the PG axis)



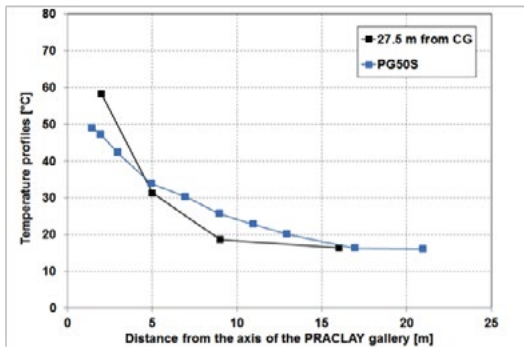
f Pore water pressure profiles in P49E (16 m from the PG axis)

Figure 3-22: Temperature and pore water pressure profiles for P38E, P42E and P49E.

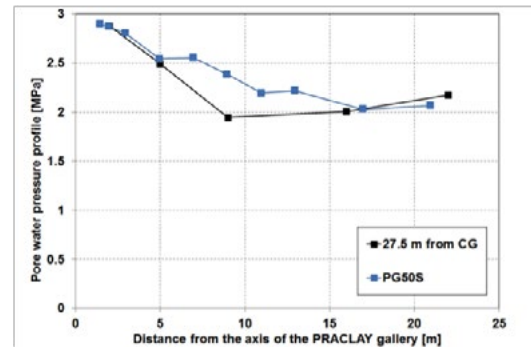
### 3.3.4. Comparison between PG50S and the Connecting gallery boreholes

To complete this section on the response of the Boom Clay, a comparison is made between the profiles obtained from the PG50S sensors and the profile gathered from the Connecting gallery boreholes (P35E, P38E, P42E, P49E) using the sensors located 27.5 m from the Connecting gallery lining (Figure 3-23(c)).

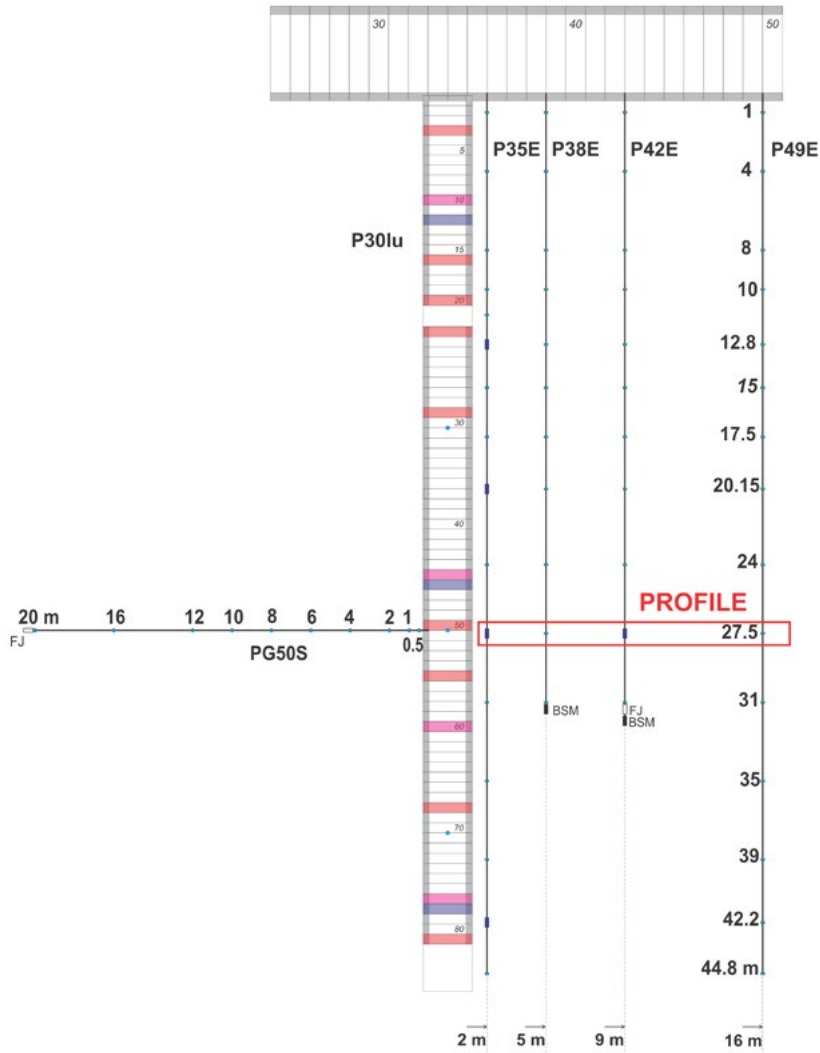
The temperature profiles (Figure 3-23(a)) show some differences: (i) a steeper temperature gradient is measured from the Connecting gallery borehole profile, and (ii) the PG50S profile shows a larger thermally affected zone (around 15 m). Conversely, the pore water pressure profiles show quite similar responses (Figure 3-23 (b)), mainly in terms of the gradient between the beginning and end of the profiles. As the temperature profile from the Connecting gallery boreholes is similar to that in PG50D (Figure 3-16, Figure 3-17 and Figure 3-18), it tends to confirm the influence on temperature of an additional heat transfer mechanism due to the open boreholes. This heat transfer mechanism is assumed to be convection.



a Temperature profiles



b Pore water pressure profiles



c Position of the profile at 27.5 m

Figure 3-23: Comparison between the profiles of temperature (a) and pore water pressure (b) in PG50S and at a distance of 27.5 m from CG at the end of the start-up phase. c) Position of the profile at a distance of 27.5 m from CG.

### 3.4. Responses in the bentonite seal

To monitor the evolution of the seal, instruments were embedded inside the bentonite block during the installation of the seal in three different sections, A, B and C (Figure 3-24). Various instruments, such as piezometers, flat-jacks and thermocouples, are installed in these sections.

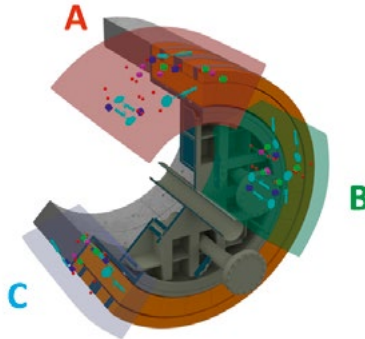


Figure 3-24: Illustration of the seal with the different sensors.

Figure 3-25 shows the evolution of the temperature for different thermocouples in section A. A temperature increase has been observed since the beginning of the heating phase, with a different evolution between TC-A15 and TCA1, TC-A11 and TC-A5. TC-A11 and TC-A1 are in fact located at the bentonite/steel flange interface in the heated part of the experiment, while the others are at the bentonite/steel flange interface at the opposite side of the heated area. At the beginning of the third phase, it was observed that the temperatures measured by thermocouples TC-A15 and TC-A5 increased faster compared with the first two phases. This observation has to be related to the installation of an insulation door in front of the seal, which contributed to a lower dissipation of the heat in the non-heated part of the PRACLAY gallery one day before the third heating phase. This will have consequences in the following observations.

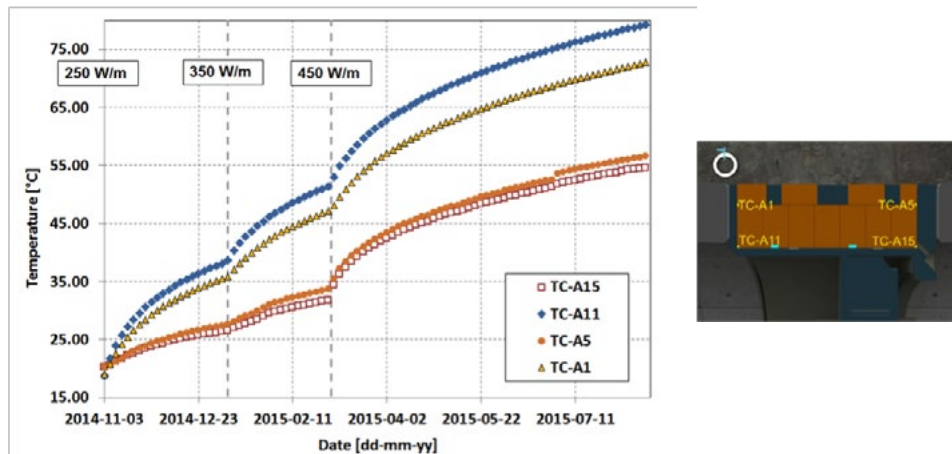


Figure 3-25: Evolution of the temperature in section A of the seal structure.

Figure 3-26 shows the evolution of the pore water pressure at the Boom Clay/bentonite interface for the three sections of the seal, and compares it with the PRACLAY gallery pore water pressure evolution. Seal PP-A1, Seal PP-B1 and Seal PP-C2 are located at the same axial (longitudinal) position in the bentonite ring. The three distinct heating phases can clearly be seen. The pore water pressure evolutions between these three sensors are very similar and smoothly follow the evolution of the pore water pressure in PG. Conversely, Seal PP-A3, which is closer to the accessible part of PG, has a lower value of pore water pressure compared with the other three. This difference reflects the role of the seal as an impervious

boundary condition limiting the increase in the pore water pressure close to the accessible gallery. As a consequence, a significant hydraulic gradient between the heated and non-heated parts of the PRACLAY gallery is created.

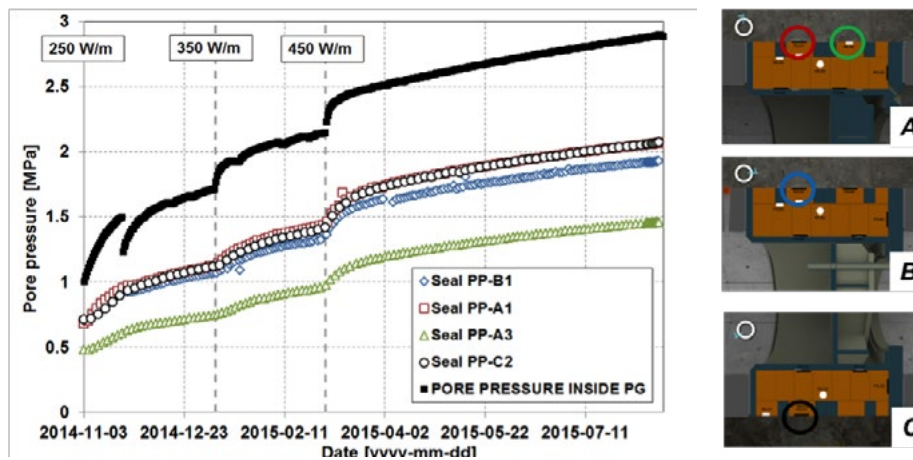


Figure 3-26: Pore water pressures at the Boom Clay/bentonite interface for the three sections, A, B and C (filters facing the Boom Clay), together with the pore water pressure inside the PG.

Figure 3-27 shows the pore water pressure measured at different positions at the top of the PG, from the heated part (Ring 21) to the accessible part (Ring 20), thereby covering the Boom Clay/bentonite interface at the seal over a total length of about 1.5 m. This Figure highlights the significant pressure gradient over this distance and confirms the low-permeability boundary condition created by the bentonite seal.

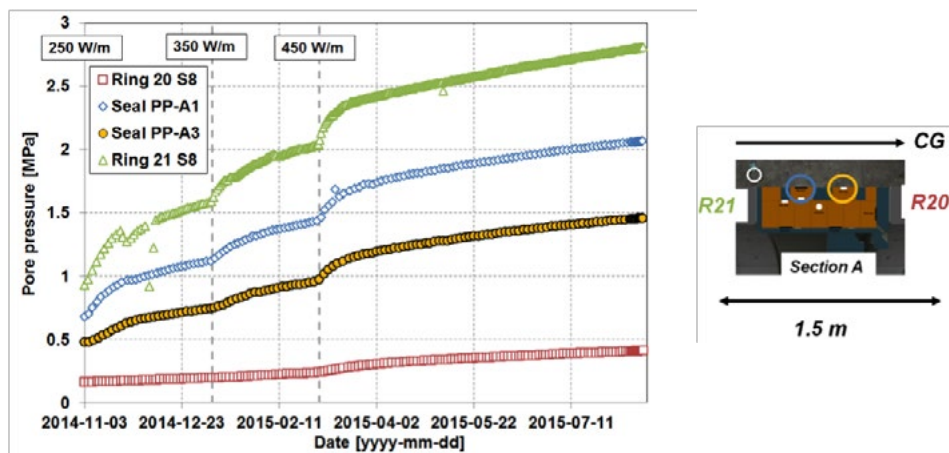


Figure 3-27: Pore water pressures measured at the Boom Clay/bentonite interface in section A and at the Boom Clay/concrete lining interface in Ring 21 and Ring 20. All sensors are located at the top of the gallery, facing the Boom Clay.

Figure 3-28 shows the pore water pressure inside the bentonite ring measured inside section B. The Seal PP-B2 sensor started to increase at the beginning of July 2015, meaning that the bentonite is saturating at this position on the ring.

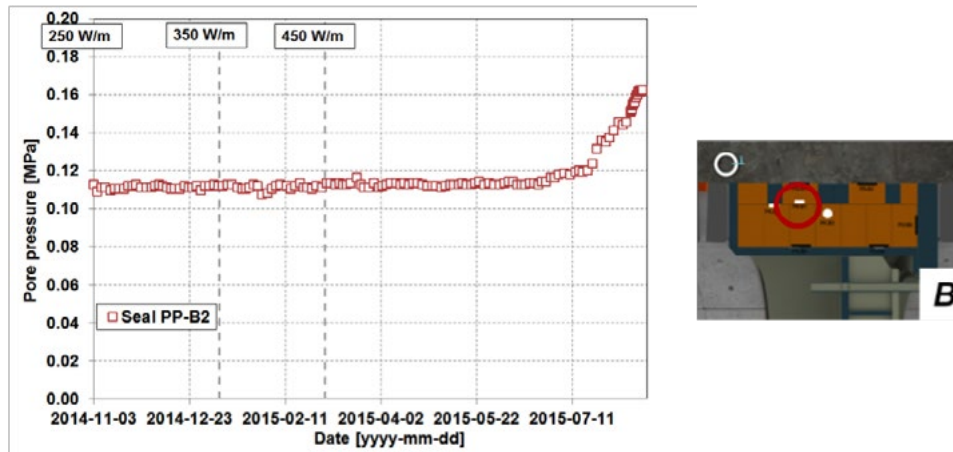


Figure 3-28: Evolutions of the pore water pressures inside the bentonite ring (Seal PP-B2 filter).

Figure 3-29 shows the pore water pressure at the interface between the steel cylinder and the bentonite ring. When heating first started, a very slight increase in pressure was observed in almost all the sensors. This slight increase was more marked for the Seal PP-A5, Seal PP-A7 and Seal PP-B5 sensors in sections A and B. At the beginning of the third phase, a higher increase rate could be observed for all the sensors, mainly explained by the installation of the insulation door, which allows the temperature to increase more inside the seal structure. Seal PP-A5 records the largest increase compared with the other sensors; greater hydration at this position on the seal is likely to occur.

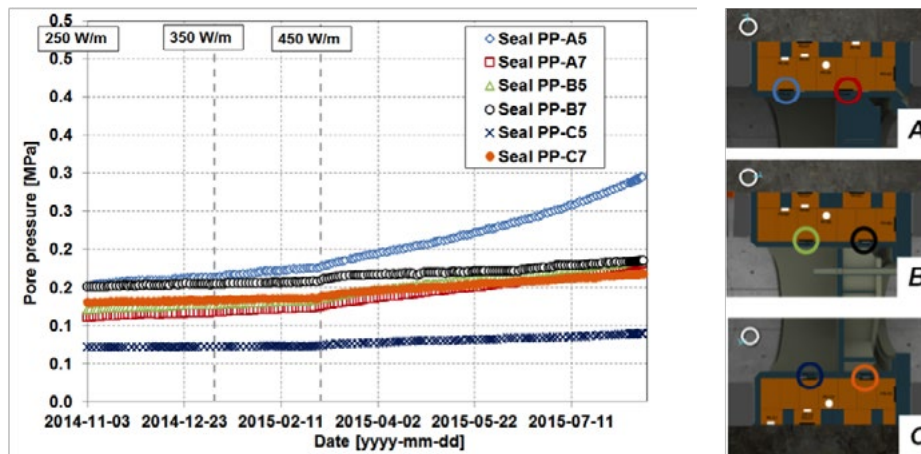


Figure 3-29: Evolution of the pore water pressure at the interface between the steel ring and the bentonite.

Figure 3-30 and Figure 3-31 show the evolution of the total pressure at the Boom Clay/bentonite interface (radial) and at the bentonite/steel downstream flange interface (axial), respectively. For all sections, the total radial pressure, against the Boom Clay, showed a small evolution after the heater switch-on. The effect of the insulation door produced a small increase around the beginning of the third phase. Unfortunately, Seal PG-PG-A1 failed early in July.

The total axial pressure shows a somewhat similar evolution, with a small increase at the beginning of the heating followed by an almost constant or even decreasing trend for section A. A small pressure increase related to the combined effect of the door installation and the power rise was observed at the start of the third heating phase.

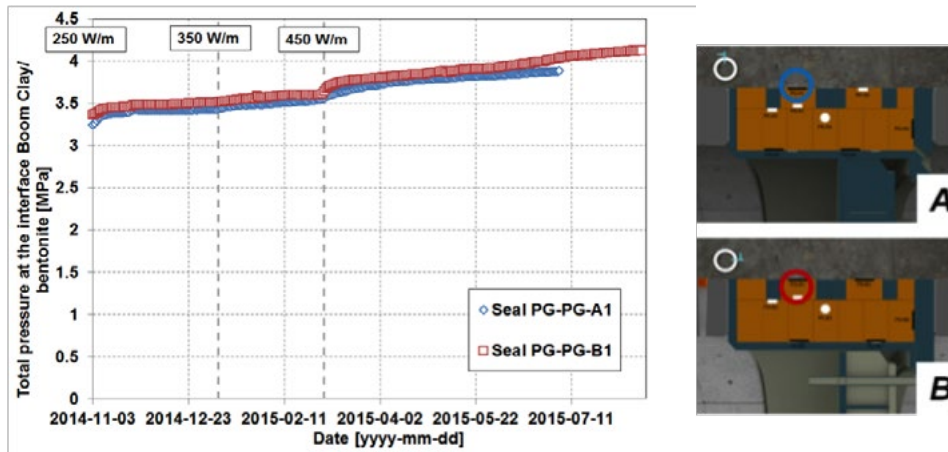


Figure 3-30: Total radial pressure at Boom Clay/bentonite interface.

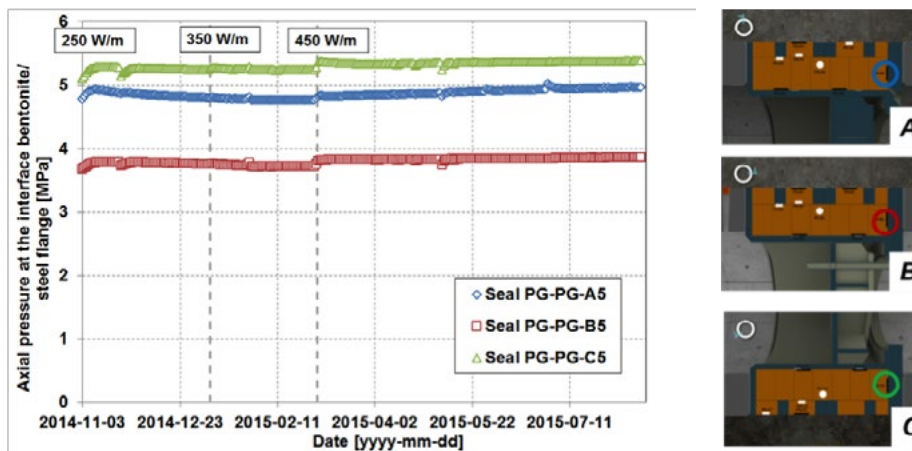


Figure 3-31: Total axial pressure at the bentonite/steel flange interface.

The displacement of the seal towards the Connecting gallery is monitored by a total station, which is able to determine the distance between its position and the position of the prisms. The results of this follow-up are shown in Figure 3-32. Since heating began, all four prisms on the seal have undergone homogeneous displacement. Since the insulation door was installed in front of the seal, the measurements have shown some variations due to the presence of the door. Nevertheless, the trend in the displacement can still be observed and at 80°C an overall displacement of about 10 mm is obtained for the different points.

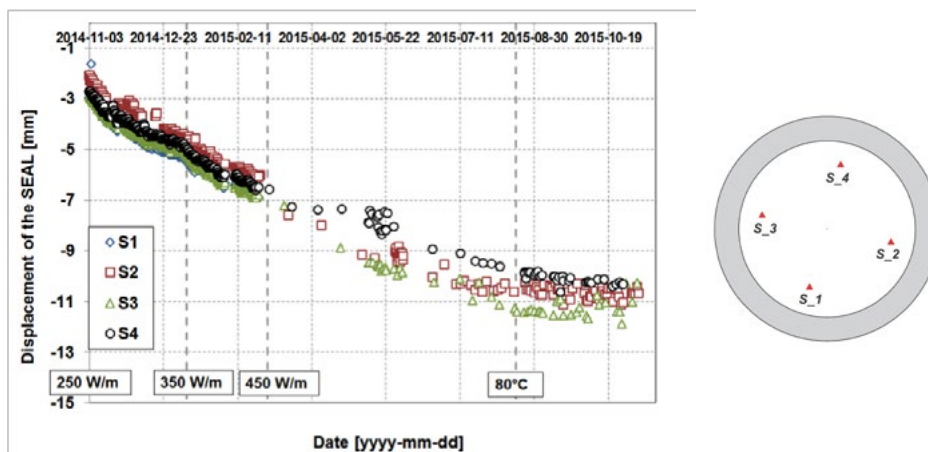


Figure 3-32: Displacement of the seal structure since the start of heating (negative displacement towards CG).

### 3.5. Responses in the concrete lining

#### Total pressure against the lining

Three lining rings (R12, R46 and R78) have been instrumented with total pressure cells. These are installed on the outside of four segments (S2, S4, S6 and S8) and measure the total pressure exerted by the Boom Clay on those rings (Figure 3-33).

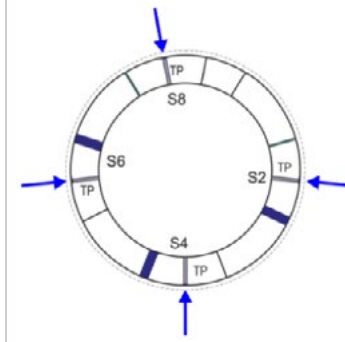
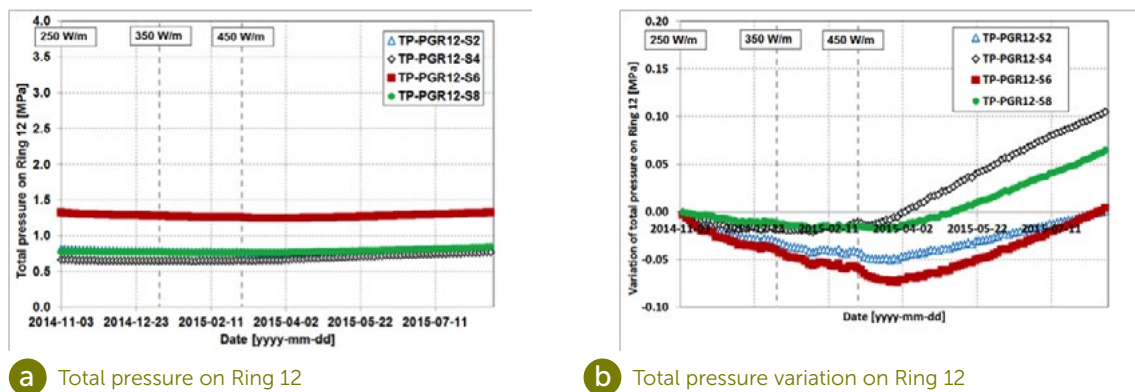


Figure 3-33: Layout of the instrumentation of the segmental concrete lining equipped with total pressure flat-jacks.

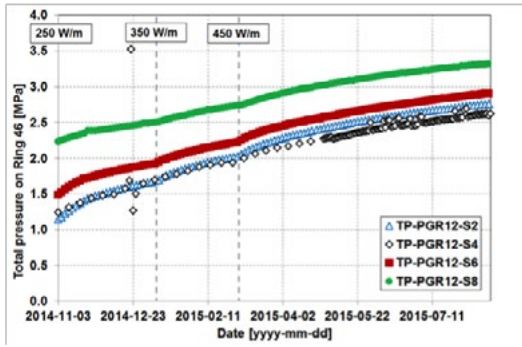
Figure 3-34, Figure 3-35 and Figure 3-36 show the total pressure and its variation with respect to the start of heating against the concrete lining during the start-up phase. In the accessible part of the PRACLAY gallery (PG12), the pressure cells indicate a slight decrease in the total pressure followed by an increase in pressure (Figure 3-34). In the heated part, total pressures directly increase similarly to the PG pore water pressure and with more pronounced variations than in the non-heated part (Figure 3-35 and Figure 3-36). The same pressure increase, between 1 and 2 MPa, is observed for all the flat-jacks of PG78, as well as for the flat-jacks associated with segments S2 and S4 of PG46. However, the pressure increase slightly differs in segments S2 and S8 of PG46: the pressure variation measured on S2 is higher than for the other three sensors and the total pressure variation on S8 is the lowest among the four sensors.



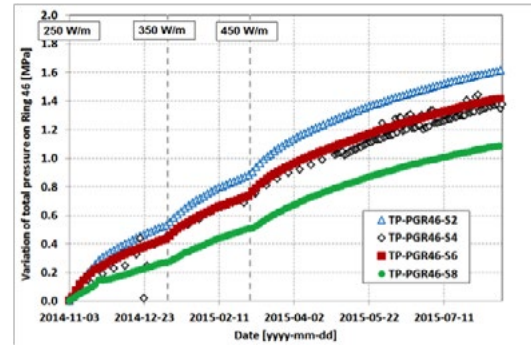
a Total pressure on Ring 12

b Total pressure variation on Ring 12

Figure 3-34: Evolution of the total pressure variation on the four flat-jacks of PG12.

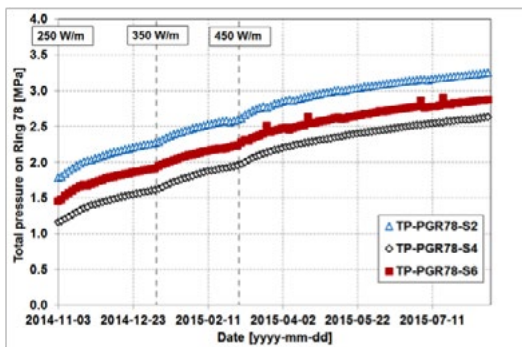


a Total pressure on Ring 46

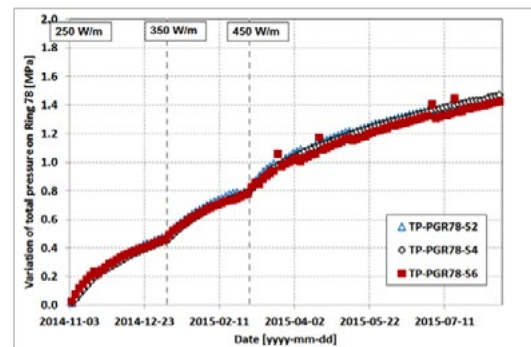


b Total pressure variation on Ring 46

Figure 3-35: Evolution of the total pressure variation on the four flat-jacks of PG46.



a Total pressure on Ring 78



b Total pressure variation on Ring 78

Figure 3-36: Evolution of the total pressure variation on the four flat-jacks of PG78.

### Circumferential stresses inside the lining

In addition to the radial pressure cells on the lining, load cells (Figure 3-37) have been installed in the same rings to monitor the loads that the segments are exerting on each other; these measurements are shown in Figure 3-38 to Figure 3-40. This measurement corresponds to an average stress because the surface area of the load cells is comparable to the contact area between two segments.

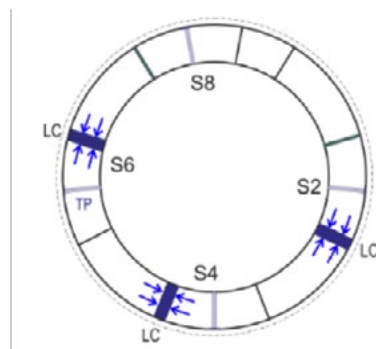
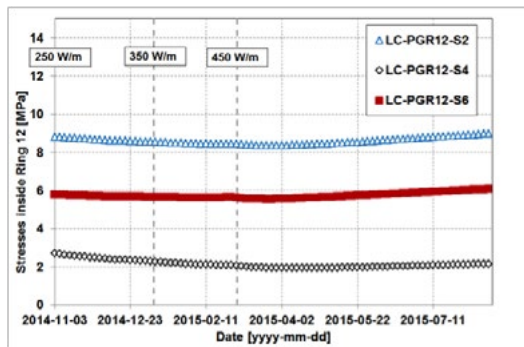


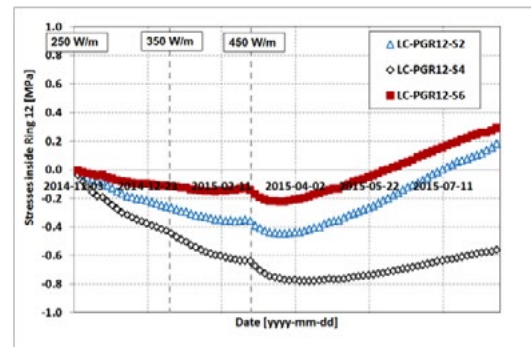
Figure 3-37: Layout of the instrumentation of the segmental concrete lining equipped with load cells.

The average circumferential stress inside PG-R12 (accessible part of PG) and its variation are shown in Figure 3-38. As for the evolution of the total pressure against the lining on Ring 12, a decrease in the stresses was observed during the first months of heating. This was followed by an increase in stress a few weeks after the third heating phase. Stress evolutions show different variations for each load cell;

nevertheless, the effect of the sudden pore water pressure drop inside the PRACLAY gallery (22 November 2014) was observed by all these sensors.



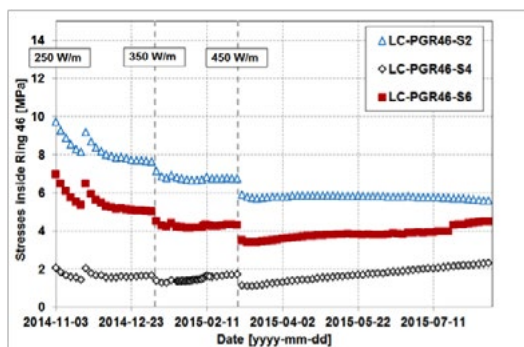
a Stresses in the concrete lining Ring 12



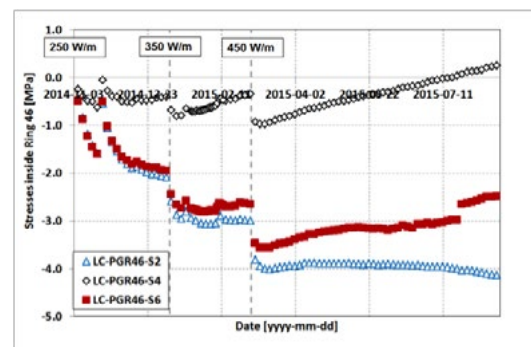
b Variation of stresses in the concrete lining Ring 12

Figure 3-38: Evolution of circumferential stresses inside PG12 since the start of heating.

Figure 3 39 shows the evolution of the average circumferential stress and its variation inside PG46 since heating began. At each new heating phase, the sudden increase in pore water pressure in PG causes a rapid decrease in the circumferential stresses inside the segments. Then, as the pore water pressure evolution in PG tends to stabilise, circumferential stresses inside the segments level off or increase slowly with time.



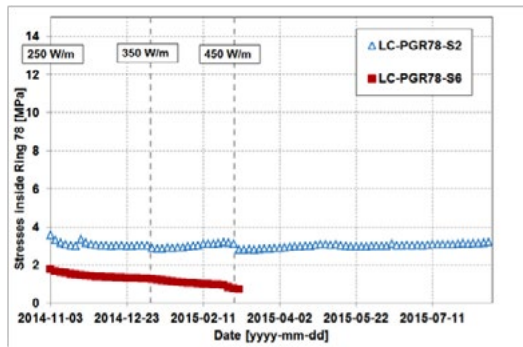
a Stresses in the concrete lining Ring 46



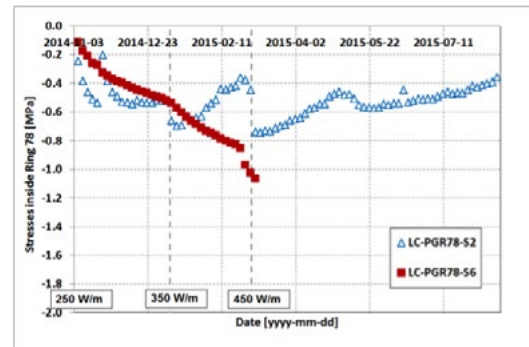
b Variation of stress in the concrete lining Ring 46

Figure 3-39: Evolution of the circumferential stresses in the lining PG46.

The evolution of the average circumferential stress and its variation inside PG78 (Figure 3 40) shows a similar pattern to what was observed with PG46: a rapid decrease in the stress is observed at the beginning of each heating phase. This drop is then reversed with a new increase in stress, which eventually stabilises.



**a** Stresses in the concrete lining Ring 78



**b** Variation of stress in the concrete lining Ring 78

Figure 3-40: Evolution of the circumferential stresses in PG78.

### 3.6. Summary

This section presents the main observations from the PRACLAY Heater test during the start-up phase. It can generally be stated that the system as a whole reacted as expected.

Based on the evolutions of the test-control parameters (temperature in the lining, at the interface with the Boom Clay and the backfill pore water pressure) and the responses of the Boom Clay, the bentonite seal and the concrete lining, the situation can be summarised as follows:

- The temperature has increased as expected in the Boom Clay, the concrete lining and the seal structure. A thermally affected zone of about 10 m around the PRACLAY gallery is observed (without considering any artefacts).
- An excess pore water pressure is generated in the backfilled part of the gallery and in the Boom Clay as a consequence of the thermal dilation coefficient between the liquid and the solid. The extent of the hydraulically affected zone varies from 10 to up to 15 m around the PRACLAY gallery, without considering the unreliable sensors from PG50D.
- The evolution of the temperature and the excess pore water pressure around the PRACLAY gallery can be described as homogeneous, without considering the end effects.
- The seal is performing as expected, allowing a good hydraulic cut-off between the heated and non-heated parts of the experiment. The high pressure inside the gallery is maintained and no leakage either from the seal or at the interface with the Boom Clay has been observed.
- The observed evolution pattern of the circumferential stresses in the concrete lining is the result of the evolution of the pore water pressure inside the gallery and of the external forces applied on the concrete lining rings.

## 4. Comparison with numerical modelling (blind predictions)

In section 4, an initial comparison is made between the observations obtained to date and the expected values from the modelling performed before the switch-on, i.e. blind predictions. The likely causes of the observed deviations and possible improvements to the models are discussed.

### 4.1. Description of the two numerical models

Two reference cases for the PRACLAY Heater test and the PRACLAY Seal test were modelled. These were based on a two-dimensional plane strain (2D-PS) model and a two-dimensional axisymmetric model (2D Axisymmetric), respectively. The basic information about these two models is introduced here in terms of geometry, boundary conditions and material properties.

The two models simulate the evolution of the PRACLAY tests since the PRACLAY gallery excavation until the end of the heating phase. In this report, the focus will be on a comparison between the experimental and the numerical results during the start-up phase (80°C). The finite element code “Code\_Bright”, developed by the Universitat Politècnica de Catalunya (UPC-BarcelonaTech), is used.

#### Geometry

The test geometry and the detailed test procedures to the best of our knowledge are considered. The two models are:

- (1) 2D Axisymmetric model (2D-Axis, Figure 4-1), which includes the geometry of almost all the components. Both the Heater test and the Seal test can be simulated in one single model. However, the anisotropic behaviour of the Boom Clay cannot be represented in this model due to the latter's induced symmetry.
- (2) 2D Plane Strain model (2D-PS, Figure 4-2): the geometry of this model consists in a cross-section perpendicular to the PRACLAY gallery axis. This geometry includes the backfill sand of the PRACLAY gallery and the concrete lining. This model could consider the anisotropic behaviour of the Boom Clay and is most representative of a cross-section at the middle of the heated part of the PRACLAY gallery. The dissipation of heat and pore water flow perpendicular to the model is not allowed with this configuration.

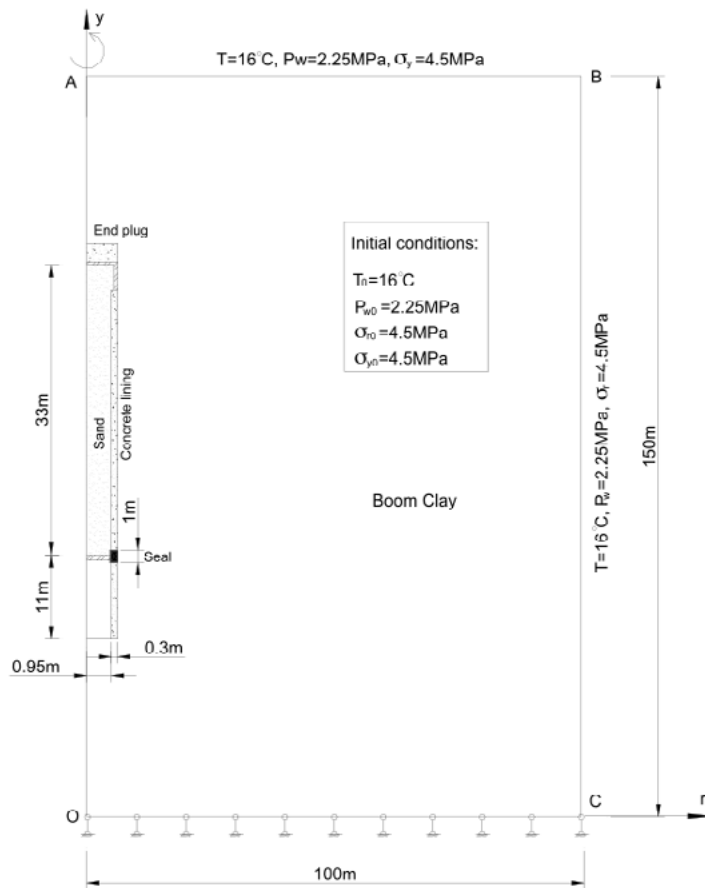


Figure 4-1: Description of the geometry of the 2D Axisymmetric model with all the components (seal, concrete lining, sand, Boom Clay). The boundary and initial conditions are described.

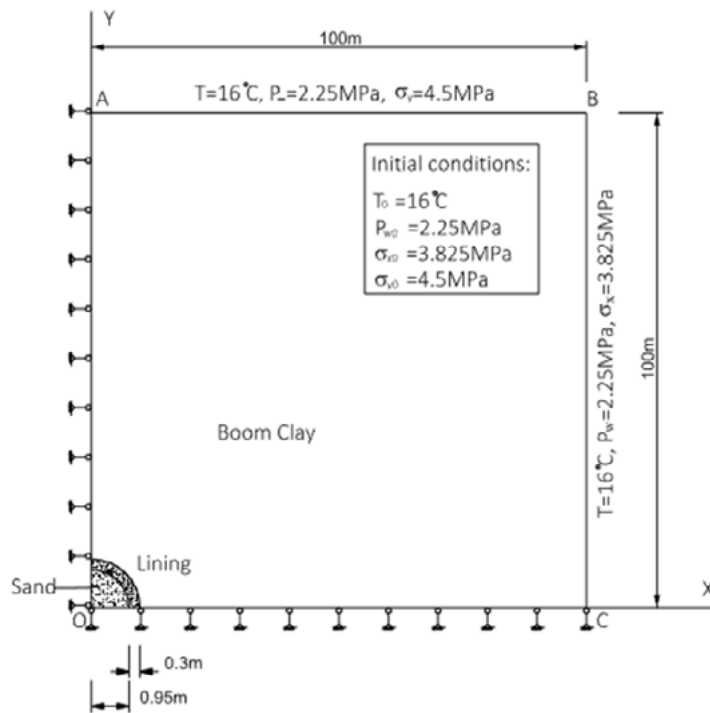


Figure 4-2: Description of the geometry of the 2D Plane Strain model with the different components (sand, lining, Boom Clay). The boundary and initial conditions are described.

### Initial conditions

The initial conditions of the modelling depend on the geometry and are described in the following tables. An isotropic value of the total stress is considered for the 2D Axisymmetric model, while a vertical and a horizontal total stress is imposed for the 2D Plane Strain model. A coefficient of earth pressure at rest ( $K_0$ ) of 0.7 is used.

		2D Axisymmetric	2D Plane Strain
Pore water pressure [MPa]	$P_w$	2.25	2.25
Total stress [MPa]	$\sigma$	4.5	
Vertical total stress [MPa]	$\sigma_v$		4.5
Horizontal total stress [MPa]	$\sigma_h$		3.825
Temperature [°C]	$T$	16	16

Table 4-1: Initial conditions for the Boom Clay for both models (based on Bernier et al., 2003; Dehandschutter et al., 2004; Bernier et al., 2007; Cornet, 2009).

		Concrete lining	Backfill sand	Bentonite (MX80)
Pore water pressure [MPa]	$P_w$	0.1	0.1	- 67*
Total stress [MPa]	$\sigma$	0.1	0.1	0.1
Temperature [°C]	$T$	16	16	16

\*Based on measurements performed by CEA and EURIDICE

Table 4-2: Initial conditions for the concrete lining, backfill sand and bentonite (MX80).

### Thermo-hydro-mechanical parameters

The main thermo-hydro-mechanical (THM) parameters of the materials (Boom Clay, sand, concrete lining and bentonite) are determined based on an extensive literature review, laboratory test results and in-situ measurements. The heat transfer is modelled using Fourier's law of conduction. The flow of water is reproduced using the classic Darcy's law. The thermo-hydraulic properties are defined in the tables below for the different materials, Table 4-3 for the Boom Clay and Table 4-4 for the other components.

		2D Axisymmetric	2D Plane Strain
Porosity [-]	$n$	0.39	
Intrinsic permeability [m <sup>2</sup> ]	$k$	4.5x10 <sup>-19</sup>	
Vertical intrinsic permeability [m <sup>2</sup> ]	$k_v$		3x10 <sup>-19</sup>
Horizontal intrinsic permeability [m <sup>2</sup> ]	$k_h$		6x10 <sup>-19</sup>
Thermal conductivity [W/mK]	$\lambda$	1.53	
Vertical thermal conductivity [W/mK]	$\lambda_v$		1.31
Horizontal thermal conductivity [W/mK]	$\lambda_v$		1.65

Table 4-3: Main thermo-hydraulic properties of the Boom Clay (based on Horseman et al., 1987; Bernier et al., 2003; Bastiaens et al., 2006; Chen et al., 2011; Chen, 2012; Garitte et al., 2014; Chen et al., 2014).

		Bentonite	Sand	Concrete lining
Initial porosity [-]	$n$	0.396*	0.394	0.1
Intrinsic permeability [m <sup>2</sup> ]	$k$	2.2x10 <sup>-21</sup>	2.3x10 <sup>-11</sup>	4.5x10 <sup>-18</sup>
Thermal conductivity [W/mK]	$\lambda$	0.3 (dry) -> 1.3 (saturated)	2.90	2.86

\*Based on measurements performed by CEA and EURIDICE

Table 4-4: Main thermo-hydraulic properties of the sand, bentonite and concrete lining. These materials are supposed to be isotropic in the different models (based on Davey, 1954; Mitchell, 1956; Powell et al., 1966; Borgesson and Hernelind, 1999; Chapuis, 2004; Bamforth et al., 2008; Chen and Ledesma, 2009; Chen and Li, 2011).

With regard to the mechanical behaviour of the different components considered in the models, an elasto-plastic model using a Drucker-Prager criterion with a hardening behaviour of the effective friction angle is used for the Boom Clay. The Boom Clay has been modelled assuming the apparition of an excavation-damaged zone (EDZ) with a certain extension around the PG. In this zone, the properties have been modified in order to consider the damage caused by excavation, which was determined on the basis of in-situ measurements of pore water pressure variation after excavation. Beyond this zone, the properties of the intact Boom Clay are considered. The modification of the parameters mainly concerns the elastic properties. The mechanical properties are given in the following table (Table 4-5).

		Intact Boom Clay (undamaged zone)	Damaged zone
Isotropic elastic modulus [GPa]	$E$	1.05	0.3
Poisson's ratio [-]	$\nu$	0.125	
Vertical elastic modulus [GPa]	$E_v$	0.7	0.2
Horizontal elastic modulus [GPa]	$E_h$	1.4	0.4
Shear modulus [GPa]	$G_v$	0.28	0.08
Poisson's ratio [-]	$\nu_{hh}$	0.25	
Poisson's ratio [-]	$\nu_{vh}$	0.125	
Effective cohesion [MPa]	$c'$	0.3	
Initial effective friction angle [°]	$\phi'_{initial}$	5	
Final effective friction angle [°]	$\phi'_{final}$	18	
Dilatancy angle [°]	$\psi$	0	

Table 4-5: Mechanical properties of the Boom Clay (based on Bernier et al, 2003; Bernier et al., 2007; Dizier, 2011; Chen et al., 2011; Chen, 2012).

The bentonite inside the seal is modelled considering the Basic Barcelona Model (BBM), taking into account the variation of the suction. In order to keep this report as clear as possible, the mechanical properties of the bentonite are not given here. This information is available in several scientific publications (Tang, 2005; Gatabin et al., 2006; Villar, 2008). The concrete lining and the backfill sand are assumed to behave elastically. The following table gives an overview of the mechanical properties of the sand and of the concrete lining. In the model, the three different types of concrete used to build the gallery (Van Marcke et al., 2013) are considered, as can be seen in the following table.

		Sand	Concrete lining
Elastic modulus [GPa]	$E$	0.03	27 (C30/37) 44 (C80/95) 55 (C125/50)
Poisson's ratio [-]	$\nu$	0.2	0.2

Table 4-6: Mechanical properties of sand and concrete lining (based on Bamforth et al., 2008).

## 4.2. Comparison with the observations

### 4.2.1. Test-control parameters

#### Temperature in the concrete lining segments

Figure 4-3 gives a comparison between the measurements and the 2D Axisymmetric numerical predictions of the temperature evolution at the intrados (inner surface, Figure 4-3(a)) and at the extrados (outer surface, Figure 4-3(b)) of the four segments (S2, S4, S6 and S8) of PG50 before reaching 80°C on the temperature indicator. The agreement for S4, S6 and S8 is good. The predictions in S2 are higher than observed with a maximum difference of 13°C.

The difference between S2 and the other segments is assumed to be due to a convection cell in the

horizontal borehole, as explained in the previous section. This presumed additional heat transfer mechanism is not considered in these modellings.

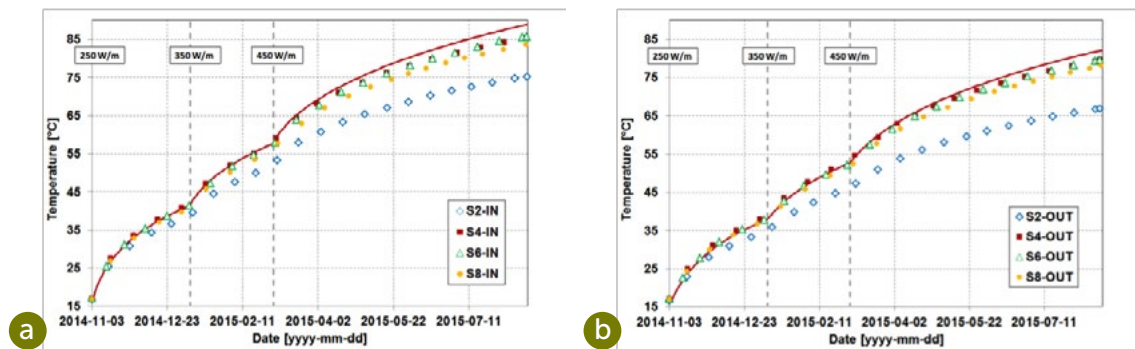


Figure 4-3: Temperature inside the concrete segments of Ring 50 since start-up of heating. Comparison with the 2D Axisymmetric model (red curve) at the intrados (a) and at the extrados (b).

Figure 4-4 shows the four temperature longitudinal profiles measured along the intrados of the four concrete lining segments (S2, S4, S6 and S8) of the rings when the target temperature of 80°C is reached, compared with the numerical results.

From these comparisons, it can be observed that:

- The modelled temperature agrees quite well with the longitudinal profiles along S2 (except in R50), S4 and S6.
- At the top of the gallery, small differences between numerical and experimental results are observed for S8. Close to the seal a significant deviation is also noticed between the experiment and the model; the temperature is largely underestimated in the model.

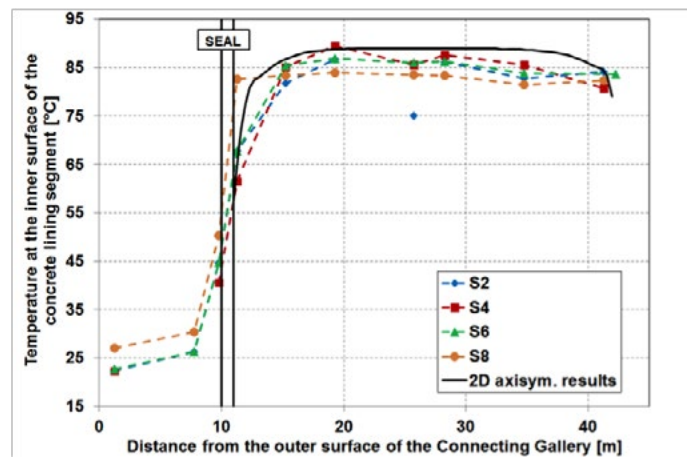


Figure 4-4: Longitudinal profiles of temperature along the intrados of backfilled PG when temperature indicator reached 80°C (measurements vs model predictions with 2D-Axis model).

The difference between the measured and the modelled temperature in the top segments of the PRACLAY gallery might be explained by considering the possibility that the gallery was not fully backfilled with sand. In fact, close to the seal structure, it was extremely difficult to inject the sand and it is most likely that a zone was not entirely filled. As a consequence, the top part of the PRACLAY gallery may be composed of pure water or a mixture of water and very loose sand. The heat transfer properties of the backfilled PRACLAY gallery could be altered by the existence of such a zone.

### Pore water pressure inside the PRACLAY gallery

The pore water pressure inside the PRACLAY gallery is an important hydraulic boundary for the PRACLAY Heater test, and the degree of agreement between its measured and predicted values may directly affect the prediction of thermo-hydro-mechanical responses in the surrounding materials. Figure 4-5 gives a comparison of the pore water pressure inside the PG, between the measurements and the predictions with the two models (2D-PS and 2D-Axis). The overall agreement can be considered to be good for these two models. The sudden drop in the pore water pressure inside the PRACLAY gallery that occurred on 22 November 2014 was not considered.

During the period from 13 to 19 January 2015, a few litres of water leaked through the seal. In order to check the sensitivity of our models, this leakage was modelled (Figure 4-6). It can be observed that modelling can accurately reproduce the measured variation trend in the pore water pressure in the PRACLAY gallery due to the leakage, which increases confidence in the modelling of the pressure inside the gallery. Indeed, the evolution of this pressure depends on several factors such as: saturation degree of backfill materials, compressibility and thermal dilation coefficient of pore fluid and of the solid phase, stiffness and transmissivity of the concrete lining, etc. Moreover, it can be seen that the effect of this leakage on the pore water pressure vanishes after several weeks (dotted red line versus continuous red line), which suggests that such a small leakage has no significant influence on the overall behaviour of the experiment.

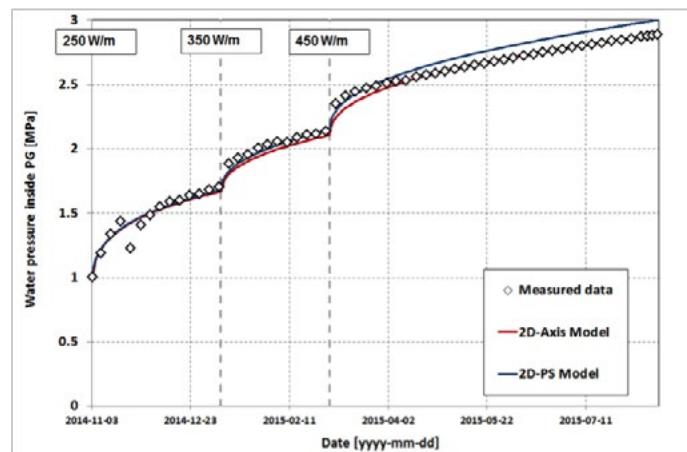


Figure 4-5: Comparison of the pore water pressure inside the PG between measurements and predictions with the two different models.

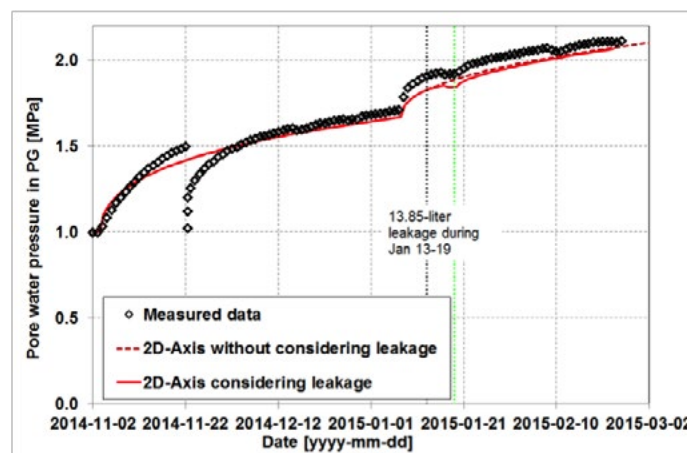


Figure 4-6: Comparison between the experimental and the numerical results of the pore water pressure evolution in the backfill sand. Modelling considered the effect of the leakage through the fibre optics.

## 4.2.2. Observations in the Boom Clay

This section considers the comparison of the numerical results with the observations in the Boom Clay. First, the evolution of temperature and pore water pressure is described according to the different models. Then the different profiles are presented and discussed, but only for the 2D-PS due to the anisotropic properties of the Boom Clay.

### 2D Axisymmetric results: evolution of temperature and pore water pressure

Figure 4-7 and Figure 4-8 show the experimental evolution of the temperature and the pore water pressure compared with the modelling results in PG50D and PG50S. It can be observed that the modelled temperature is in good agreement for PG50D (Figure 4-7(a)) but not for PG50S (Figure 4-8(a)). In fact, the modification of the heat transfer around this borehole due to the open casing is not considered in our models, in which only heat transfer by conduction is specified.

In terms of pore water pressure, it can be seen that the evolution is quite well reproduced by the model for both boreholes (Figure 4-7(b) and Figure 4-8(b)).

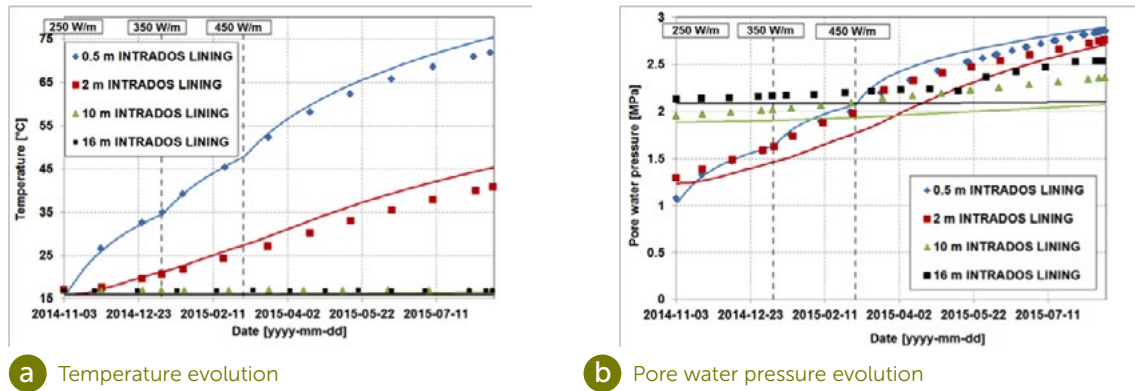


Figure 4-7: Comparison between numerical (continuous curve) and experimental (points) evolution of the temperature and pore water pressure in PG50D for the 2D Axisymmetric model.

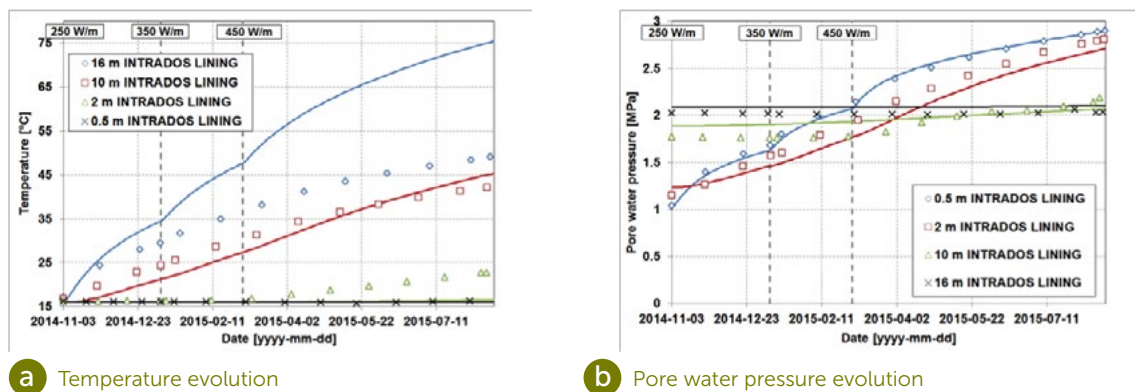


Figure 4-8: Comparison between numerical (continuous curve) and experimental (points) evolution of the temperature and pore water pressure in PG50S for the 2D Axisymmetric model.

## 2D-PS results: evolution of temperature and pore water pressure

Figure 4-9 and Figure 4-10 show the comparison of the temperature and pore water pressure evolution using the 2D-PS model. As with the 2D Axisymmetric model, it can be observed that the agreement is quite good for both the temperature and the pore water pressure evolution in PG50D. Conversely, no agreement can be found when comparing the evolution of the temperature in PG50S due to the presence of open boreholes and heat transfer by convection, as discussed previously.

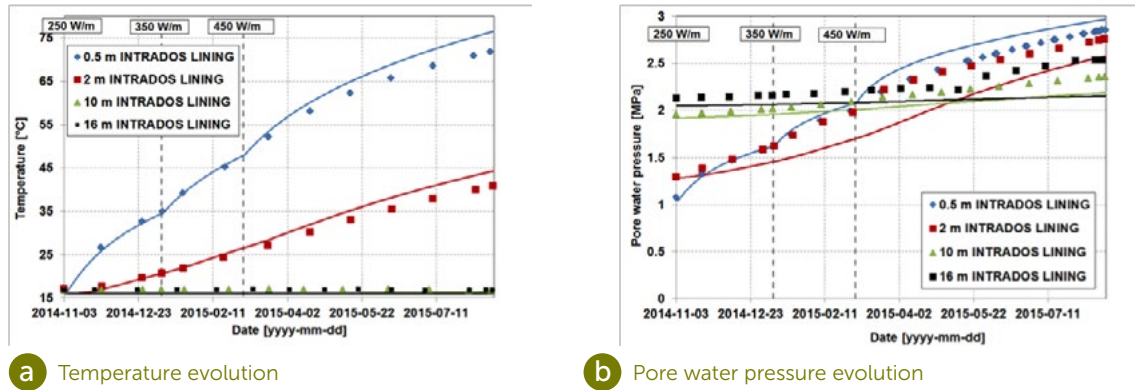


Figure 4-9: Comparison between numerical (continuous curve) and experimental (points) evolution of the temperature and pore water pressure in PG50D for the 2D-PS model.

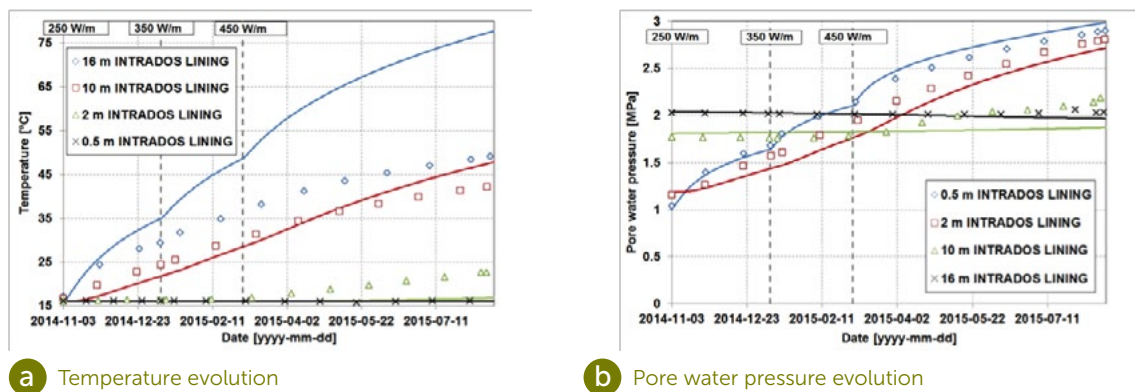


Figure 4-10: Comparison between numerical (continuous curve) and experimental (points) evolution of the temperature and pore water pressure in PG50S for the 2D-PS model.

It has already been shown that the pore water pressure in the horizontal plane first manifests a slight decrease after increasing power, similar to the observations in the ATLAS test. This is assumed to be the consequence of the mechanical anisotropic properties of the Boom Clay. While this phenomenon was correctly reproduced numerically for the ATLAS test, this is not the case for the present predictions of the PRACLAY Heater test, as can be seen in Figure 4-11, which shows the evolution of the pore water pressure on two sensors located at the same distance from the PRACLAY gallery in two different boreholes (PG50S and PG50D).

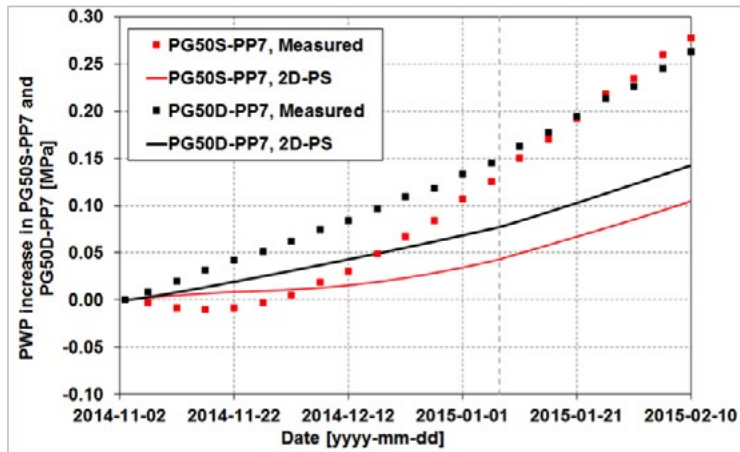


Figure 4-11: Comparison of the experimental and numerical (2D-PS) evolution of the pore water pressure for PG50S-PP7 and PG50D-PP7 located at a distance of 4 m from the intrados of the PG.

### Temperature and pore water pressure profiles

The experimental temperature profiles compared with the modelling results are shown in Figure 4-12. Figure 4-12(a) and Figure 4-12(b) correspond to the temperature profiles in PG50D and PG50S, respectively, while Figure 4-12(c) is the profile with the sensors installed in boreholes P35E, P38E and P42E, which are drilled from the Connecting gallery and located about 27.5 m from this gallery and thus around PG50.

The different profiles are taken at three different times: at the end of 250 W/m, at the end of 350 W/m and at the end of 450 W/m when a temperature of 80°C was reached at the Boom Clay/concrete lining interface. As before, quite good agreement is obtained for PG50D, while the model cannot match the temperature profiles in PG50S. However, the temperature profiles obtained with the sensors from the Connecting gallery are in good agreement with the models. This confirms that the measurements in the horizontal boreholes drilled from the PG are an artefact.

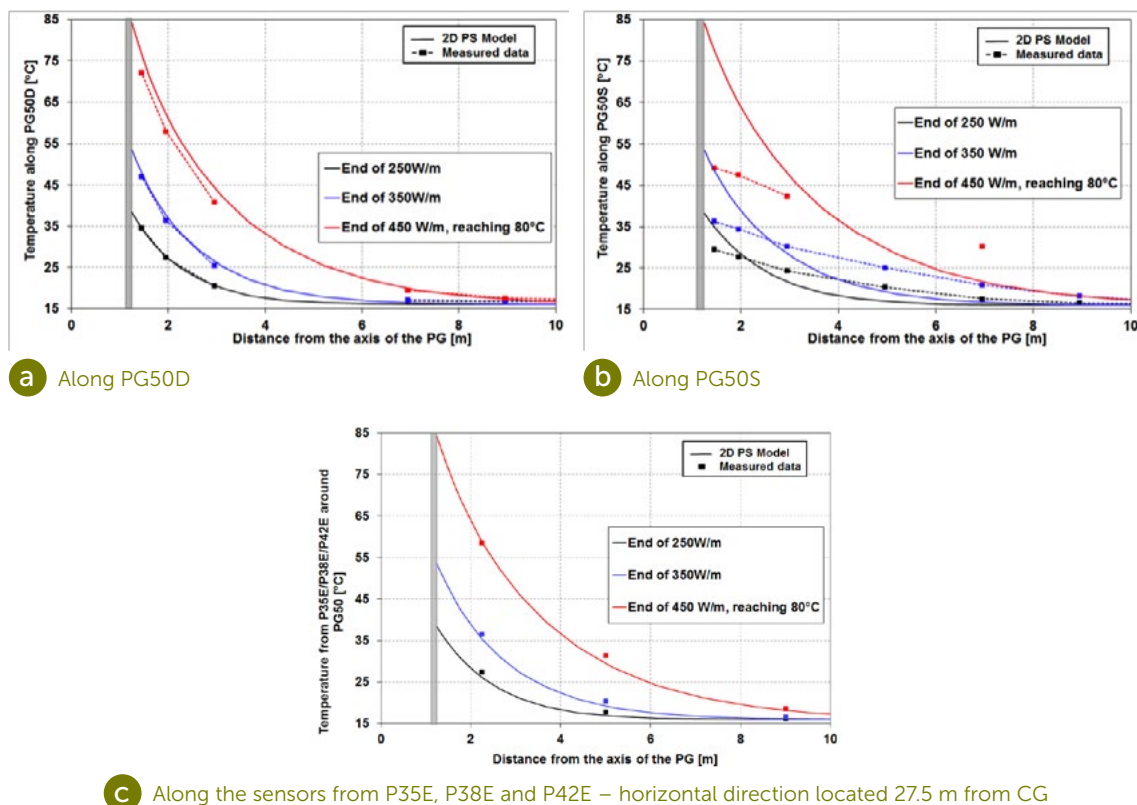


Figure 4-12: Comparison between the experimental and numerical temperature profiles around PG50.

Figure 4-13 shows the comparison between the numerical and experimental profiles of pore water pressure around PG50, i.e. in PG50D, in PG50S and with the installed sensors in P35E, P38E and P42E located 27.5 m from the CG. Four profiles have been considered: before the switch-on and, as before, at the end of 250 W/m, at the end of 350 W/m and at the end of 450 W/m when the target temperature of 80°C is reached at the Boom Clay/concrete segment lining interface.

From these comparisons, it can be observed that:

- The modelled PWP gradient over the lining is quite different from the measured one. In fact, a more pronounced transition in the pore water pressure field is observed in the model closer to the concrete lining.
- Modelling can correctly reproduce the trend in the pore water pressure evolution after heating; however, it underestimates the increase in the Boom Clay pore water pressure in the near field. Furthermore, the modelled pore water pressure in the far field of the Boom Clay does not match well in PG50D. The experimental values at this position are, however, doubtful, as seen in the observations section.

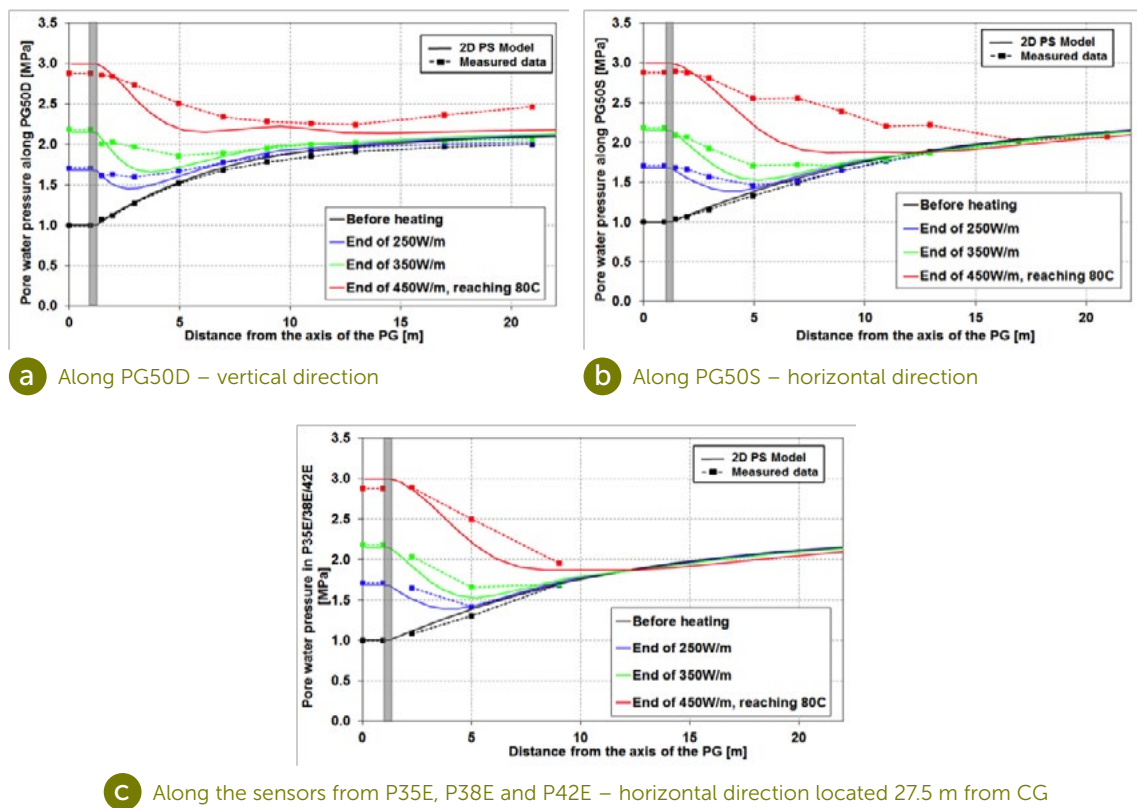


Figure 4-13: Comparison between the experimental and numerical profiles of pore water pressure around PG50.

#### 4.2.3. Observations in the seal and concrete lining structures

##### Stresses and pore water pressure in the seal

Figure 4-14 shows a comparison between the experimental and the 2D Axisymmetric numerical results in the seal structure and at the Boom Clay/bentonite interface.

The numerical results of the pore water pressure at the Boom Clay/bentonite interface indicate that

the model underestimates the variation in pressure at this interface for the sensors located either close (Seal PP-A1, Seal PP-B1 and Seal PP-C2) or not (Seal PP-A3) to the heating part of the experiment (see Figure 4-14(a)).

In terms of the total pressure variation at the Boom Clay/bentonite interface, Figure 4-14(b) shows that the model underestimates the variation in the total radial pressure.

Furthermore, although the model predicts an increase in the axial pressure since heating was applied at the interface between the downstream flange and the bentonite, this swelling is not observed, as can be seen in Figure 4-14(c).

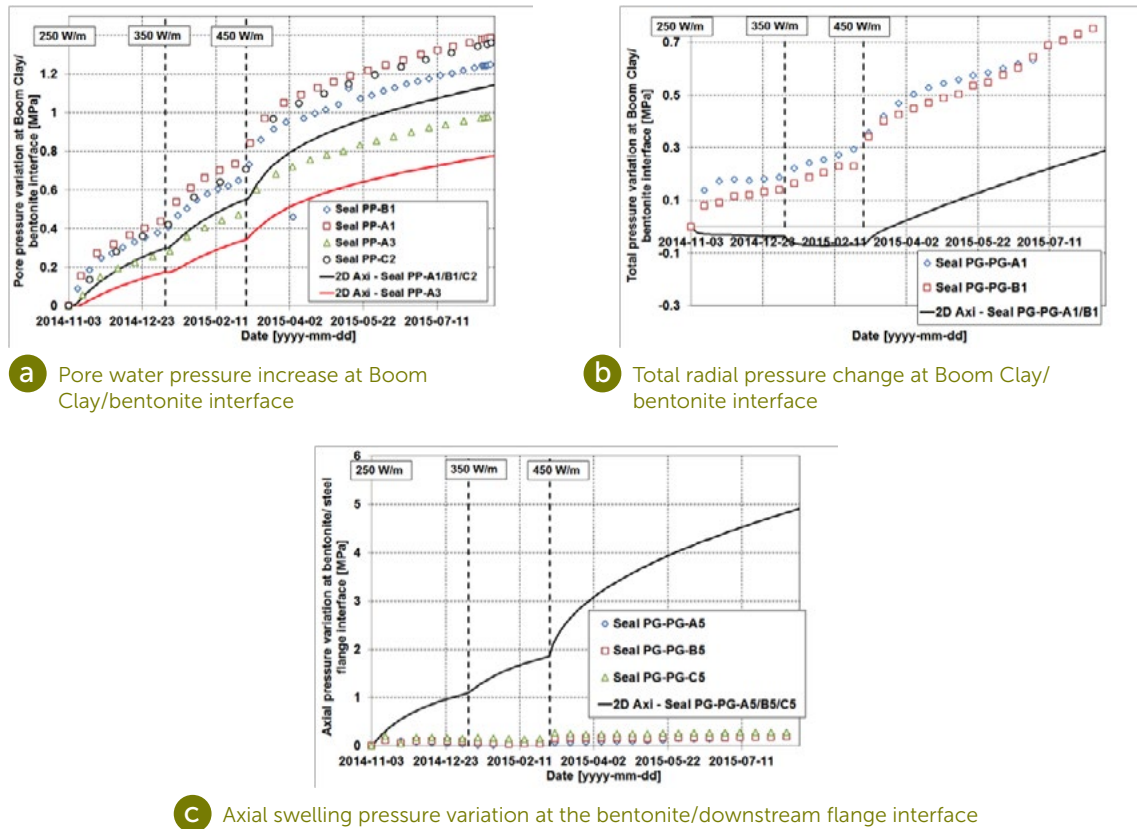


Figure 4-14: Pore water pressure and total radial pressure at the bentonite/Boom Clay interface and axial swelling pressure against the flange. Comparison with the 2D-Axis numerical results.

### Stresses and total pressure at the concrete lining/Boom Clay interface

Measured circumferential stresses and total pressure at the Boom Clay/concrete lining interface in PG46 are compared with numerical results in Figure 4-15 and Figure 4-16, respectively. The modelling results are based on both the 2D-PS model and the 2D Axisymmetric model for the comparison.

Overall, the modelling results fall within the range of the measured results, and the evolution trend and the variation amplitude are well reproduced. However, it is important to mention that the experimental measurements show considerable dispersion from one segment to another, which does not allow for a straightforward interpretation.

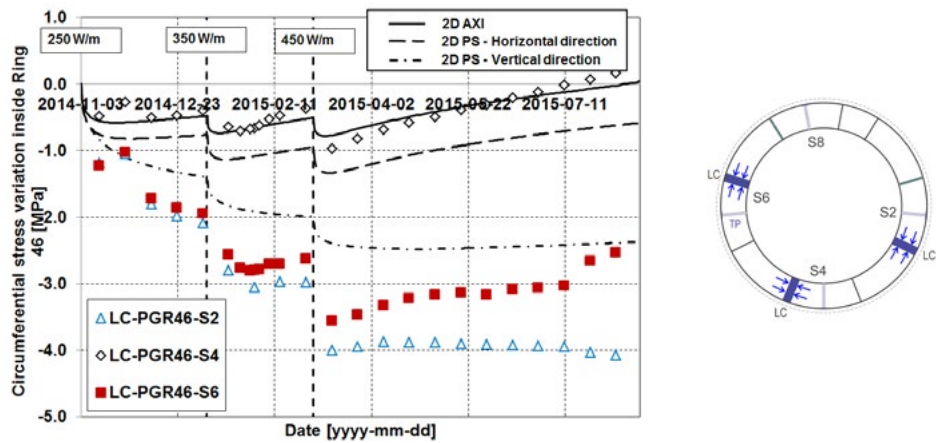


Figure 4-15: Circumferential (hoop) stress variation between concrete segments in PG46. Comparison with the modelling results. 2D PS-Hor refers to the modelled circumferential stress relative to the horizontal direction, while 2D PS-Vert refers to the modelled circumferential stress in the vertical direction.

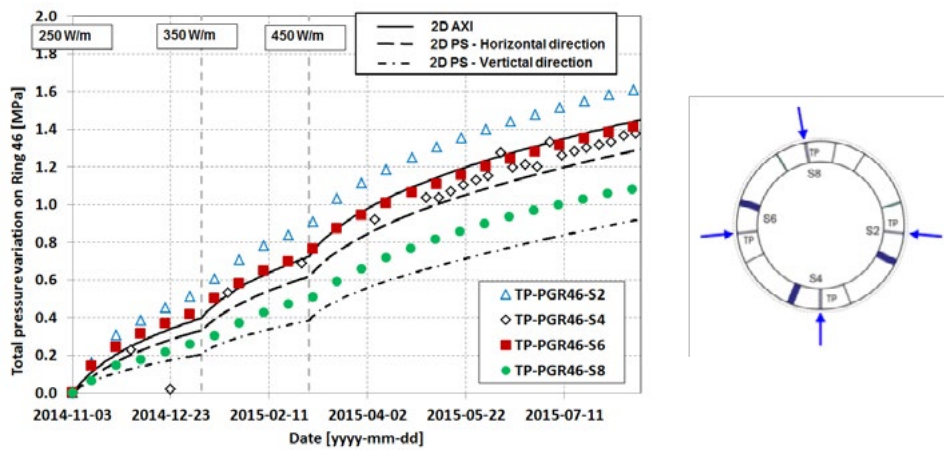


Figure 4-16: Total pressure measurement at Boom Clay/lining interface on PG46. Comparison with the modelling results. 2D PS-Hor refers to the modelled total pressure relative to the horizontal direction, while 2D PS-Vert refers to the modelled total pressure in the vertical direction.

### 4.3. Summary and future work

Comparisons between the blind predictions and the measurements obtained during the start-up phase of the PRACLAY Heater test show that most of the measured temperatures in the concrete lining segments, the seal and the Boom Clay agree well with the predictions, except that:

- The modelled temperatures in S2 of the lining of Ring 50 deviate substantially from the observations due to the presence of the open borehole.
- The modelled temperatures in the Boom Clay along the horizontal boreholes drilled from PG30S, PG50S and PG70S from the PRACLAY gallery deviate from the measurements.
- The predicted temperature at section A of the seal is much lower than the measured one.

The above-mentioned deviations are most probably due to the enhanced heat transfer by water convection inside horizontal boreholes PG30S, PG50S and PG70S, which was not considered in the model.

Numerical predictions can reproduce well the trend in the pore water pressure evolution, but underestimate the magnitude of the variation, especially in the near field of PG. The modelling cannot accurately capture the pore water pressure gradient over the lining either. Consequently, numerical improvement is necessary in the future. This can be done by incorporating various aspects, such as:

*(1) Considering a more realistic intrinsic permeability of the lining:*

The lower pore water pressure gradient obtained by numerical prediction depends on the overall intrinsic permeability of the concrete lining, which was assumed to be one order of magnitude higher than that of the Boom Clay in the modelling. The present comparisons assumed that the overall intrinsic permeability of the concrete lining might be lower. In fact, because of the thermal expansion of the rubber between joints and the creep behaviour of the Boom Clay, it might be expected that the joints between the rings are now filled with Boom Clay and are becoming less and less permeable.

*(2) Giving greater consideration to the permeability evolution around PG:*

Studying the permeability evolution in the EDZ is actually one of the objectives of the PRACLAY Heater test.

*(3) Refining the coupled THM constitutive laws and associated parameters to better model the coupled THM behaviour of the Boom Clay, especially for the near-field responses.*

Unlike the ATLAS experiment, which is representative of the far-field THM behaviour of the Boom Clay, the PRACLAY Heater test deals with both the near field and the far field behaviour of the Boom Clay. Anisotropic behaviour in the near field is, for instance, expected to be more complex than that in the far field.

Finally, even though the seal behaviour is a secondary objective of the PRACLAY experiment, comparison between the measurements and the predictions shows that its general behaviour is not yet fully understood and needs further investigation. A more detailed analysis of all aspects of seal behaviour will come within the scope of a future report.

## 5. Conclusions

This report gives initial insight into the test evolution during the start-up phase of the PRACLAY Heater test, i.e. until the average target temperature of 80°C was obtained. To reach this target temperature, three heating phases were applied; one at 250 W/m, a second at 350 W/m and a third at 450 W/m. An extensive network of instrumented boreholes and instruments in the seal, lining and gallery registered the response of the experimental set-up and the surrounding Boom Clay. The different components of the experiment (Boom Clay, concrete lining and seal) reacted to heating more or less as predicted. Most of the instruments functioned properly; some failed (e.g. the strain gauges inside the concrete segments) and were abandoned.

**Inside the PRACLAY gallery**, the temperature and pore water pressure immediately started to increase after the switch-on of the heating system. The pore water pressure evolved from 1 MPa just before the start of heating to 2.9 MPa at the end of the start-up phase.

In the **Boom Clay**, the dissipation of heat caused an increase in temperature and pore water pressure. It was shown that the thermally affected zone had extended about 10 m around the PRACLAY gallery by the end of the start-up phase. The hydraulically affected zone extended 10 to 15 m around the PG.

In the **seal structure**, the pore water pressure started to increase at the Boom Clay/bentonite interface, with higher pressure close to the heated part of the PG. The total pressure at the Boom Clay/bentonite interface and inside the bentonite ring showed a response to the heating phase. Moreover, the monitored displacement of the seal structure shows a uniform displacement towards the Connecting gallery. The different observations leave no doubt about the performance of the seal, which serves as hydraulic cut-off between the heated and the non-heated part, avoiding dissipation of pore water pressure between the heated and non-heated parts of the experiment.

Within the **concrete lining**, a variation in total pressure was observed, caused by the combined effect of the pressure variation inside the PRACLAY gallery and the total pressure modification acting on the rings.

From a **modelling** point of view, the comparisons of the measurements with the 2D axisymmetric and 2D plane strain models show that the temperature and pore water pressure correspond quite well with the blind predictions in the gallery and in the Boom Clay. Deviations between the measurements and the predictions of temperature in horizontal or upward boreholes are almost certainly related to the presence of open boreholes, allowing a potential heat transfer by convection in the casing. This results in a modification of the temperature field around the boreholes. For the seal, a larger dispersion between the measurements and the modelling was observed. A more detailed analysis of the complex seal behaviour will be conducted in the future course of the experiment. The conclusions of this initial comparison of the measurements with the numerical results give us a first indication of how and where to improve the models used for the future follow-up of the experiment during the ten-year heating phase at a constant temperature at the interface with the Boom Clay.

Overall, it can be stated that the first phase of the experiment is a success, with the whole system reacting to the start-up phase and evolving as expected. Since 19 August 2015, the temperature at the interface between the lining and the Boom Clay has been maintained constant at 80°C.



## 6. References

- Baldi G., Hueckel T., Peano A., Pellegrini R., 1991. Developments in modelling of thermo-hydro-mechanical behaviour of Boom Clay and clay-based buffer (vol.2). Commission of the European Communities. Nuclear Science and Technology EUR 13365/2.
- Bamforth P., Chisholm D., Gibbs J., Harrison T., 2008: Properties of Concrete for use in Eurocode 2
- Bastiaens W., Bernier F., Li X.L., 2006. An overview of long-term HM measurements around HADES URF. In: EUROCK 2006 multiphysics coupling and long term behaviour in rock mechanics, 15–26.
- Bel J., Bernier F., 2001. Temperature Criterion Related to Clay Based Backfill Materials in the Framework of a Geological Repository of Heat Producing Radioactive Waste (HLW). Proc. ICEM'01, The 8th International conference on Environmental Management, Bruges, Sept.30 - Oct.4
- Bernier F., Li X.L., Verstricht J., Barnichon J.D., 2003. CLIPEX: Clay Instrumentation programme for the EXTension of an underground research laboratory. EC contract FI4W-CT96-0028. Final report, Commission of the European Communities. Nuclear Science and Technology EUR 20619.
- Bernier F., Li X.L., Bastiaens W., 2007. Twenty-five years' geotechnical observation and testing in the Tertiary Boom Clay formation. *Géotechnique*, 57(2): 229–37.
- Bernier F., Li X.L., Bastiaens W., Ortiz L. et al. 2007. SELFRAC : Fractures and self-healing within the excavation disturbed zone in clays. Final report. Euridice report December 2007.
- Borgesson L., Hernelind J., 1999. Coupled thermo-hydro-mechanical calculations of the water saturation phase of a KBS-3 deposition hole. Technical Report TR-99-41.
- Chapuis R.P., 2004. Predicting the saturated hydraulic conductivity of sand and gravel using effective diameter and void ratio. *Canadian Geotechnical Journal*, 41(5): 787–795.
- Chen G.J., Ledesma A., 2009. Coupled thermo-hydro-mechanical modeling of the full scale in-situ test "Prototype Repository". *Journal of Geotechnical and Geoenvironmental Engineering, ASCE*, 135(1), 121-132.
- Chen G.J., Li X.L., 2011. Numerical modeling of PRACLAY Seal test. Internal report.
- Chen G.J., Sillen X., Verstricht J., Li X.L., 2011. ATLAS III in situ heating test in Boom Clay: Field data, observation and interpretation. *Computers and Geotechnics*, 38(5), 683-696.
- Chen G.J., 2012: Modeling of PRACLAY tests: improved HM parameters of Boom Clay based on in-situ measured PWP around PG, SAC 41 meeting.
- Chen G.J., Maes T., Vandervoort F., Sillen X., Van Marcke P., Honty M., Dierick M., Vanderniepen P., 2014. Thermal Impact on Damaged Boom Clay and Opalinus Clay: Permeameter and Isostatic Tests with  $\mu$ CT Scanning. *Rock Mechanics and Rock Engineering*, Volume 47(1), 87-99.
- Coll C., 2005. Endommagement des roches argileuses et perméabilité induite au voisinage d'ouvrages souterrains. Thèse de doctorat de l'Université Joseph Fourier- Grenoble 1.

- Cornet F.H., 2009. In situ Stress measurement campaign at SCK•CEN Underground Laboratory by Ecole et Observatoire des Sciences de la Terre, Université de Strasbourg, Internal report.
- Davey N., 1954. Concrete mixes for various building purposes, Proc. of a symposium on mix design and quality control of concrete, Cement and Concrete Assn. London, 28-41.
- De Bruyn D., Labat S., 2002. The second phase of ATLAS: the continuation of a running THM test in the HADES underground research facility at Mol. Engineering Geology, 64(2), 309-316.
- Dehandschutter B., Vandycke S., Sintubin M., Vandenberghe N., and Wouters L., 2004: Brittle fractures and ductile shear bands in argillaceous sediments: inferences from Oligocen Boom Clay (Belgium). Journal of Structural Geology 27, 1095-1112.
- Dizier A., 2011. Caractérisation des effets de température dans la zone endommagée autour des tunnels de stockage de déchets nucléaires dans des roches argileuses. PhD thesis, Université de Liège.
- Gatabin C., Touze G., Billaud P., Imbert C., Guillot W., 2006. ESDRED PROJECT-MODULE 1, Selection and THM characterisation of the buffer material. Technical Report E.NT.0GME.05.0005/B.
- Garitte B., Gens A., Vaunat J., Armand G., 2014. Thermal Conductivity of Argillaceous Rocks: Determination Methodology Using In Situ Heating Tests. Rock Mechanics and Rock Engineering, Volume 47(1), 111-129(19).
- Horseman S.T., Winter M.G., Entwistle D.C., 1987. Geotechnical characterisation of Boom Clay in relation to the disposal of radioactive waste. Final report, Commission of the European Communities. Nuclear Science and Technology EUR10987.
- Le T.-T., 2008. Comportement thermo-hydro-mécanique de l'argile de Boom. PhD thesis, CERMES, Ecole Nationale des Ponts et Chaussées, Paris.
- Mitchell L.J., 1956. Thermal properties, A.S.T.M. Ap. Tech. Publicn. No. 169, pp. 129-135.
- Powell R.W., Ho C.Y., Liley P.E., 1966. Thermal Conductivity of Selected Materials. National Standard Reference Data Series-National Bureau of Standards-8.
- Sillen X., Marivoet J., 2007. Thermal impact of a HLW repository in clay. Deep disposal of vitrified high-level waste and spent fuel. Mol, Belgium: SCK•CEN.- 59 p.- (External Report of the Belgian Nuclear Research Centre; ER-38; CCHO 2004-2470/00/01, DS 251.SAF).- ISSN 1782-2335
- Sultan N., 1997. Etude du comportement thermo-mécanique de l'Argile de Boom: Expériences et modélisation. PhD thesis, Ecole Nationale des Ponts et Chaussées.
- Tang A.M., 2005. Effet de la température sur le comportement des barrières de confinement, PhD thesis, Ecole Nationale des Ponts et Chaussées.
- Van Marcke P., Li X.L, Bastiaens W., Verstricht J., Chen G., Leysen J., Rypens J., 2013. The design and installation of the PRACLAY In-Situ Experiment. EURIDICE report 13-129.
- Villar M.V., 2005. MX-80 bentonite, thermo-hydro-mechanical characterisation performed at CIEMAT in the context of the Prototype project, CIEMAT Technical Report.





